Water Resources Research

RESEARCH ARTICLE
10.1029/2021WR031731

Explicit Incorporation of Discrete Fractures Into Pore Network Models

Chenhui Wang[1], Kejian Wu[2], Gilbert Scott[3], Alfred R. Akisanya[2], and Quan Gan[4]

[1]Research institute of petroleum exploration and development, Beijing, China, [2]School of Engineering, University of Aberdeen, Aberdeen, UK, [3]Anasuria Operating Company, Aberdeen, UK, [4]School of resources and safety engineering, University of Chongqing, Chongqing city, China

Key Points:

- A novel method (FM-PNM) is developed to incorporate discrete fractures into pore networks in both 2D and 3D models
- This method is able to efficiently simulate fluid flow properties in fractured porous media
- This method extends the scope of applications of pore network model to fractured porous media

Supporting Information:

Supporting Information may be found in the online version of this article.

Correspondence to:

C. Wang and K. Wu,
wangchenhui_upc@outlook.com;
kejian.wu@abdn.ac.uk

Citation:

Wang, C., Wu, K., Scott, G., Akisanya, A. R., & Gan, Q. (2022). Explicit incorporation of discrete fractures into pore network models. *Water Resources Research*, *58*, e2021WR031731. https://doi.org/10.1029/2021WR031731

Received 1 DEC 2021
Accepted 3 DEC 2022

Author Contributions:

Conceptualization: Chenhui Wang, Kejian Wu, Gilbert Scott
Formal analysis: Chenhui Wang
Investigation: Chenhui Wang
Methodology: Chenhui Wang
Software: Chenhui Wang, Gilbert Scott
Supervision: Kejian Wu, Gilbert Scott, Alfred R. Akisanya
Validation: Chenhui Wang, Gilbert Scott
Visualization: Chenhui Wang
Writing – original draft: Chenhui Wang
Writing – review & editing: Kejian Wu, Gilbert Scott, Alfred R. Akisanya, Quan Gan

Abstract Fractured porous media exist widely in reservoir rocks and fractures play a critical role in fluid flow processes. High resolution direct numerical simulations of fluid flow can provide important insight into pore-scale processes and flow mechanisms in fractured permeable media, however, the tremendous computational costs prevent these methods from being applied into larger scale models. Pore network modeling is an alternative solution to this problem, but currently it can only be used in porous media without fractures. This work is concerned with incorporating discrete fractures into pore network modeling to represent fractured porous media. A new fracture matrix pore network model (FM-PNM) is developed to efficiently simulate the fluid flow properties in fractures associated with the pore matrix. Discrete fractures are transformed into a fracture pipe network and integrated with the pore matrix that is represented by a network of pore bodies and pore throats. These two networks are coupled together to create a single nested network which is topologically equivalent to the fractured porous medium. This method extends the scope of applications of pore network modeling to fractured porous media. The permeability of the coupled network (FM-PNM) is benchmarked by Lattice Boltzmann simulation for various structures of pore matrix and discrete fracture networks.

1. Introduction

Fluid flow in porous media is of great importance to understand various processes in science and engineering. Fractures are ubiquitous in reservoir rocks and play a critical role in transport processes (Berre et al., 2018; Dershowitz et al., 2004; Golf-Racht, 1996; Meakin & Tartakovsky, 2009; Rouchier et al., 2012). The porous medium; or permeable medium; is the domain in which transport, chemical and mechanical processes happen. For example, reservoir rocks are porous media in which hydrocarbon flows, aquifers are porous media where fresh water resides, soils are porous media where rains penetrate for plants growth, etc (M. J. Blunt et al., 2013; Rabot et al., 2018; K. Wu et al., 2006). The typical size of void spaces in most rocks is of the order of microns. The distinctive features of fractures are their large permeability but small porosity compared to pore matrix. The permeability of the open and connected fractures is orders of magnitude higher than the matrix, making them dominate the fluid flow in many types of media. In this work, we will be concerned with pore scale modeling of the fluid flow in fractured porous media where the fractures are of similar size and comparable to the pore matrix.

With advances in computation and imaging technologies, pore scale models are increasingly being developed to study the mechanisms of fluid flow in permeable media (M. J. Blunt, 2001; M. J. Blunt et al., 2013; Bultreys et al., 2016; Flannery et al., 1987; Dunsmuir et al., 1991; Piri & Karpyn, 2007; P. Wu et al., 2020). Computational fluid dynamics (CFD) uses numerical methods to study and solve fluid flow related problems. When it comes to pore scale modeling, it is generally divided into two categories, that is, direct numerical simulation (DNS) and network model. Direct numerical simulations, such as finite element method, finite volume method and lattice Boltzmann method, can provide highly resolved insights into pore-scale processes (Latt et al., 2020; Liu et al., 2016; Prodanovic & Bryant, 2010; Raeini et al., 2012; Ramstad et al., 2010). These methods require the need to mesh the fluid flow domain where numerical simulations are conducted. Finer meshes generally produce more accurate simulation results, however, these can require significant increase in computational costs and time. Alternatively, network models that extract the equivalently representative network to the porous medium have been proposed (M. J. Blunt, 2001; Dong & Blunt, 2009; Gostick, 2017; Jiang et al., 2007; Scott et al., 2019). Network models capture the key parameters of the porous medium, including the geometrical and topological properties, to represent the pore structure. Network models are a discretization of the porous media and can be regarded as a coarser "mesh" over the domain, which in turn makes the network method more computationally

efficient. Briefly speaking, DNS methods are more accurate than network methods but they are generally more computationally demanding, so their applications are usually confined to small scale models. The network method is more efficient, which makes it possible to simulate larger scale porous media, and handle thousands or millions of elements simultaneously. Therefore, in our current research, we adopt the network method to deal with fractured porous media because we want to apply our model to a larger domain and model complex heterogeneous systems. However, we also utilize DNS method mainly to compare and benchmark our network model.

1.1. Overview of Pore Network and Fracture Network Models

Pore network models proposed for porous media without fractures only contain pore bodies and throats. Fractures and pores both are 3D objects, however, from the conventional pore network point of view, pore bodies and throats are simplified as one dimensional tube models which can be described by radius and length, while fractures need an additional parameter since they are generally simplified into parallel plate model involving three parameters, that is, length, width and aperture. Fractures usually have complicated morphology with varying apertures along the length and width and can be partially opened or closed. Consequently, fluid flow in fractures has a different mechanisms and regimes compared with those in pores, which makes it difficult to integrate fractures into a pore network. Furthermore, the interactions between fractures and pore matrix are complex and impose additional challenges to the study of the transfer mechanisms of fluid flow between them.

Nevertheless, many researchers have tried to simulate fluid flow in fractures by network method in the last two decades (e.g., Hughes & Blunt, 2001; Jiang et al., 2017; Jing et al., 2020; Karpyn & Piri, 2007; Rabbani et al., 2020). In general, these methods can be divided into two categories and the difference lies in whether fractures are treated implicitly or explicitly.

Hughes and Blunt (2001) proposed a network method to segment fracture space into regular connected square subdomains. The fracture has variable aperture so that the square height is determined from the fracture local aperture size. On the other hand, Karpyn and Piri (2007) applied a regular rectangular "mesh" over the fracture planes and divided it into regular subdomains, which are transformed into network elements where pore bodies and throats are assigned side by side, so that the pore network is constructed within each fracture. This pore network is more like the finite difference method rather than a traditional pore network. Rabbani et al. (2020) recently proposed a triple pore network model which also considered fractures. A watershed method was employed to extract the pore network from both meso-pores and fracture space. In this case, the fracture space is transferred into irregular subdomains. These methods treat fractures implicitly and employ a traditional network method to extract the pore network from fractures.

The other approach is to treat fracture explicitly. Jiang et al. (2017) developed an algorithm to explicitly identify fractures from micro-CT images of fractured porous media. Their paper focused on the algorithm to extract medial surfaces of fractures, which were further transformed into virtual medial axes so that a pore network could be extracted for fractures by the same procedures as those of the pore matrix (Jiang et al., 2007). In fact, this is also an implicit method to extract pore network in fractures. But their explicit identification of fractures in fractured porous media is an important contribution. Recently, Jing et al. (2020) proposed a hybrid method to represent fractured porous media and simulate gas flow. They used a regular lattice network to represent the pore matrix and a fracture pipe network for the discrete fractures network. Their model is an explicit method to represent fractures. However, there is a trade-off between the lattice size of pore matrix and computational efficiency. Furthermore, it is worth mentioning the work of Weishaupt et al. (2019), who proposed a model to couple free flow and pore network model. Their free flow domain is like a kind of large fracture and a finite difference method was used to solve free flow equations. Their treatment of fracture and pore matrix connections make it possible to couple the finite difference method and pore network model. The governing flow equations can be solved in a single calculation without iterative process.

In essence, implicit representation of fractures involves a "meshing" process, for example, Hughes and Blunt (2001) applied regular square "mesh" over fractures to construct the pore network; the mesh size affects the results of the simulations. While, explicit representation of fractures involves an upscaling, for example, the fracture pipe network method. Although explicit representation also involves dividing the fracture space into flow subdomains, the number of such domains is much less than that of implicit method.

1.2. Statement of the Problem

We recently worked on the discrete fracture network (DFN) to improve its versatility and application to complex connected fractures for computing fluid flow properties of porous media. We found that discrete fractures can be well represented and simulated by the improved fracture pipe network (Wang et al., 2022). In addition, we developed a new method to extract pore networks from micro-CT and scanning electron microscopy images (Scott, 2020; Scott et al., 2019; Wang et al., 2020). This method extracts pore elements to capture the features of pore structure from the widest to the narrowest part of the pore space (pore body to pore throat), honors the topology, and does not over segment the pore space. Consequently, we believe that an improved discrete fracture pipe network can be coupled with a pore network to better represent the interactions between fractures and porous media and predict fluid flow. The current paper will show the overall procedures for developing this fracture matrix-pore network model (FM-PNM). The main difference between the current study and our previous published paper on the improved fracture pipe network model is that the current paper considers the effects of coupling pore matrix and fractures while the previous paper only deals with fractures.

The structure of this paper is as follows. In Section 2, we introduce the general procedures for constructing a FM-PNM. The difference in assigning conductance for pore matrix and fractures is discussed. In Section 3, FM-PNM is benchmarked using 2D and 3D fractured porous media. Samples from a North Sea reservoir rock with complex pore structures are used to test the effectiveness and accuracy of the developed FM-PNM. Then, the traditional pore network is used solely to extract network from fractured porous media and the results are compared to the coupling network constructed by the FM-PNM. In addition, results from pore matrix only, fractures only and both pores and fractures are presented and analyzed. The topological properties between pore matrix and fractured porous media are studied. The pros and cons of the FM-PNM are fully discussed and the key factors for representation of fractured porous media are analyzed. Finally, conclusions are summarized in Section 4.

2. Methodology

In this section, we first show the procedures to construct the fracture matrix pore network model and each step in the flowchart will be presented in detail. The key part is to identify the fracture and matrix connection elements (F/M connections). Then, the fluid flow model is presented, for example, the governing equations, initial conditions, boundary conditions, etc.

2.1. Construction of Fracture Matrix Pore Network

The general procedures to construct fracture matrix pore network are shown in the flowchart below. Typically, it is divided into three steps. The first step is to extract the pore network from fractured porous media using our new pore network extraction tool, imagenet (Scott, 2020). Here the fractures and pore matrix are treated in the same way. Next step is important as the F/M connections are identified and then all of the other elements within fractures except F/M connections are removed. Finally, the improved fracture pipe network is extracted from the discrete fracture network (Wang et al., 2022) and incorporated into the pore network by the F/M connections.

It should be noted that one procedure we presumed that has been done before constructing a FM-PNM is the transformation of a realistic fracture into an equivalent ideal discrete fracture. Fracture pipes are then extracted based on the equivalent DFN. We used idealized and smooth fractures because we focused our current study on the development of the framework for the coupling network of fracture and matrix network. The transformation of real fractures into a DFN can be our next work.

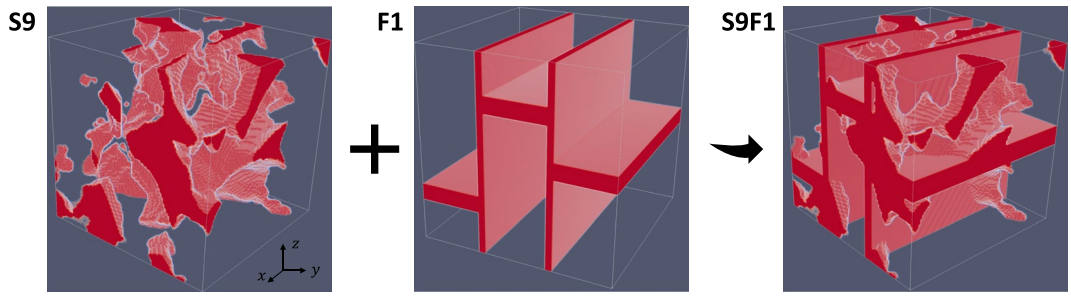

Figure 1. Illustration of a fractured porous medium, where pore space is displayed in red while solids are set as transparent. (a) Pore matrix from Berea sandstone sample S9, (b) synthetic discrete fractures F1 with rectangular shape, (c) fractured porous medium S9F1. The model size is 100^3 voxels, and the image resolution is 1μm/voxel.

Flowchart to construct fracture matrix pore network model

Input: Image of fractured porous medium
Output: The coupled network of discrete fractures and pore network

Step 1: Construct fractured porous media by incorporating discrete fracture network into pore matrix.
Step 2: Extract pore network from the above porous medium.
Step 3: Identify the F/M connection elements, and delete the other elements within fractures.
Step 4: Extract fracture pipe network from the DFN.
Step 5: Build bonds between the F/M connections and fracture centroid node to couple the two networks.

2.1.1. Extraction of Pore Network

The model used for the demonstration of the method is shown in Figure 1. The pore matrix is part of an image of Berea sandstone sample S9 that was obtained from the digital rock repository of pore scale modeling and imaging group at Imperial College London (M. Blunt & Bijeljic, 2015). The volume of the pore matrix is 100^3 voxels. To make it simple, the image resolution is assigned as 1μm/voxel so that the results can be compared with other samples. As for the discrete fractures models, five regular artificial fractures are created. Fractures apertures are of similar order of size as the pore matrix and resolution of fracture is also set as 1μm/voxel. The DFN is integrated into pore matrix to create the fractured porous medium as shown in Figure 1. Synthetic DFN is used in this study to efficiently illustrate the procedures of constructing a FM-PNM. We presume that a realistic fracture from a micro-CT image has been transformed into an equivalent discrete fracture before constructing the FM-PNM.

The first step in constructing a fracture matrix pore network is using the "imagenet" tool to extract pore network directly from the fractured porous media S9F1 (see Figure 1). The network is shown in Figure 2. The tool "imagenet" was developed by Scott (2020), which is used to perform manipulation of images and pore networks. The extraction of pore network by imagenet is a new method that overcomes many problems of the maximal ball method and medial axis method (Dong & Blunt, 2009; Jiang et al., 2007). In addition, for the 2D case, a pore network is extracted by the new pore structure quantification method, readers can refer to this paper for further information (Wang et al., 2020). However, these two methods are designed for porous media without fractures, even though they can extract a network for both matrix and fractures, they have problems when used to extract the network in fractures, which is not a good representation of the fractures by these methods. Here, we differentiate between the network in matrix and fractures. "Pore network" is used to refer to the network extracted from matrix, while "fracture pore network" refers to the network used to represent fractures. The reason to extract pore network for fracture by the "imagenet" tool is because this will facilitate the next step. In the later section, the results of the network extracted by this tool for fractured porous media will be compared with the coupled network from FM-PNM proposed in this paper.

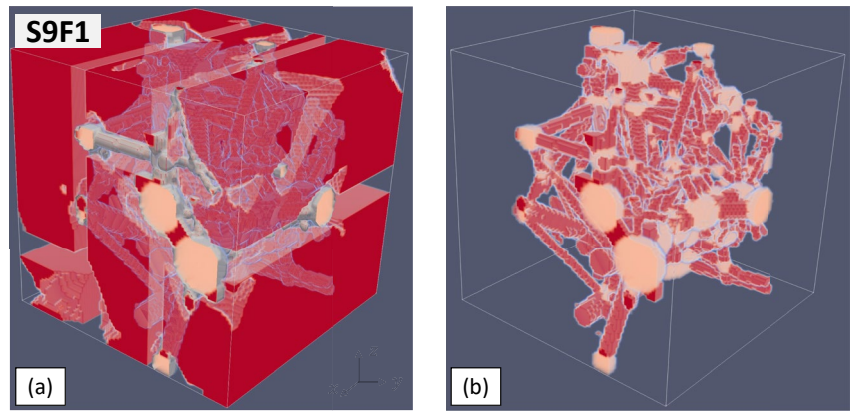

Figure 2. (a) Fractured porous media with pore network extracted by "imagenet" tool (Scott, 2020), where the solid is displayed, pore space is set as transparent and pore network is displayed inside the medium, (b) pore network for both of the fractures and pore matrix, spheres represent nodes and cylinders are bonds, both of them are referred as pore elements.

2.1.2. Identification of the F/M Connections

Two parts of the pore network generated in the first step are important and should be retained. First are the pore elements within pore matrix and second is what we called "F/M connections," which are the elements connecting fractures and pore matrix. The other redundant pore elements within the fractures are deleted. Figure 3 shows a schematic illustration of the "F/M connections." Yellow nodes residing in the fractures are "F/M connection nodes," and red bonds are "F/M connection bonds" which communicate the flow between fractures and pore matrix. The identification of F/M connections is crucial to the new method. Two features are used to distinguish the location of "F/M connections nodes." First, they locate in the void space of fracture; second, they have connections with the pore elements inside pore matrix. They are identified by the following way. First, all pore elements are divided into two groups depending on whether they reside in matrix or fractures. Second, we search all elements in fractures and check that whether they have connections with elements in matrix. If yes, F/M connection nodes are identified. Their connections with matrix are the F/M connection bonds consequently.

The reason "imagenet" tool is used for fractured porous media is that extraction of pore network by "imagenet" is based on the medial axis of pore space. Node elements are found around the branch points of the medial axis.

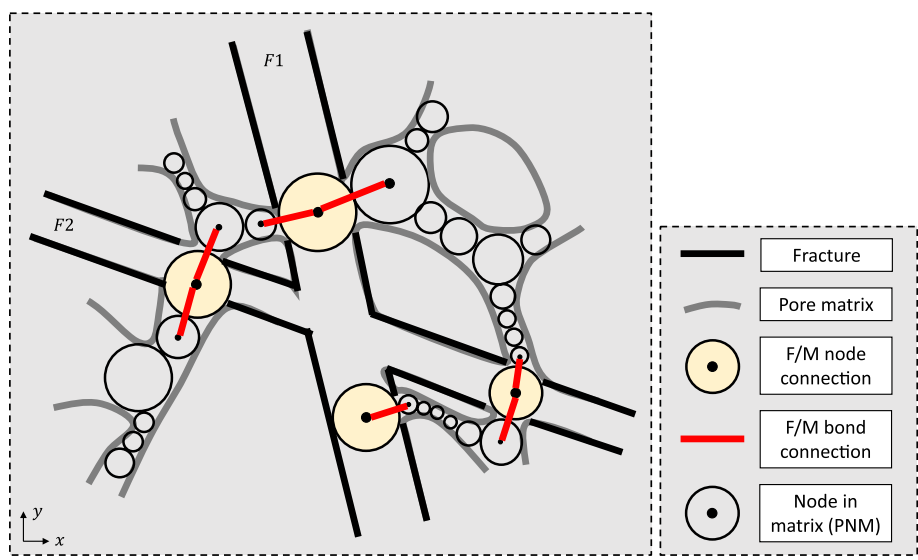

Figure 3. 2D schematic illustration of the "F/M connections," where two intersecting fractures are displayed, thick lines are boundaries between solids and matrix/fractures, circles are the pore elements used to quantify pore structure.

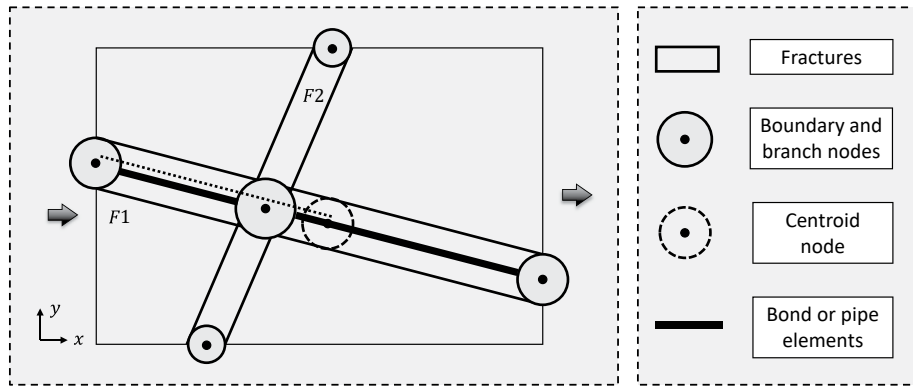

Figure 4. Illustration of 2D DFN and the representative fracture pipe network, the boundary node and branch node are used to segment fracture into pipes, dash line shows the bond repetition if boundary node is connected with centroid node.

Because branch points always exist around the position of pore matrix and fracture, this guarantees the F/M connections can be found.

2.1.3. Extraction of Fracture Pipe Network

Fracture pipe network is extracted from the discrete fracture network. Figures 4 and 5 illustrate how the fracture pipes are constructed to represent discrete fractures in 2D and 3D respectively. Fracture pipe network is equivalent to the discrete fracture network, in which the fractures are replaced with one dimensional pipe elements.

The basic procedures to build fracture pipe networks for 2D and 3D are quite similar, but there are slight differences. In the 2D case, the fracture pipe elements are constructed between the boundary nodes and branch nodes, and this idea is the same as pore network. The boundary node and branch point node split the fracture into equivalent pipes. Although fracture in 2D has a centroid, there is no need to introduce extra bonds to connect boundary node with the centroid of fracture. This avoids the repetition or overlapping of some pipe elements. As shown in Figure 4, the pipe elements with dash line are overlapped, and this could lead to extra pressure loss during fluid flow simulation. The second reason is that one pipe is enough to represent the flow in a fracture if there is no branching point between two nodes and there is no need to over segment fractures in 2D.

However, in the 3D case, the pipe elements should be connected to fracture centroid node, so that the flow subdomains can be approximately segmented. In principle, a real fracture can be extracted and represented using geometric and topological parameters, such as roughness, range of apertures, shape factor, number of nodes and bonds connected with the fracture. For the DFN in 3D case, we recently published a paper to improve the

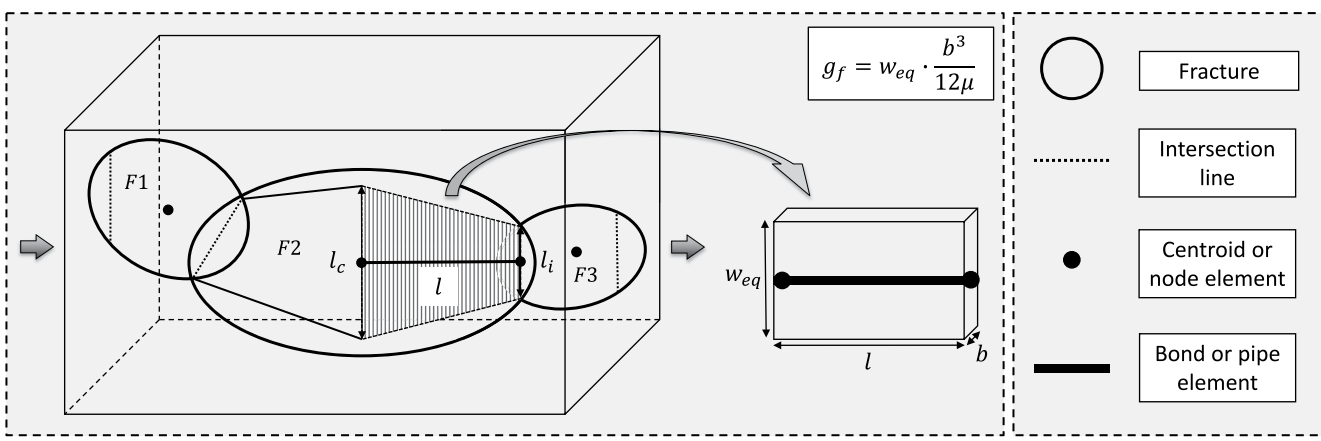

Figure 5. Illustration of the construction of the fracture pipe network from a discrete fracture network with three ellipse shape fractures (Wang et al., 2022). The shaded zone is transformed into equivalent seepage subdomain and then represented by a fracture pipe element, where g_f is the hydraulic conductance of the equivalent fracture, b, w_{eq}, l are the fracture aperture, equivalent width and length.

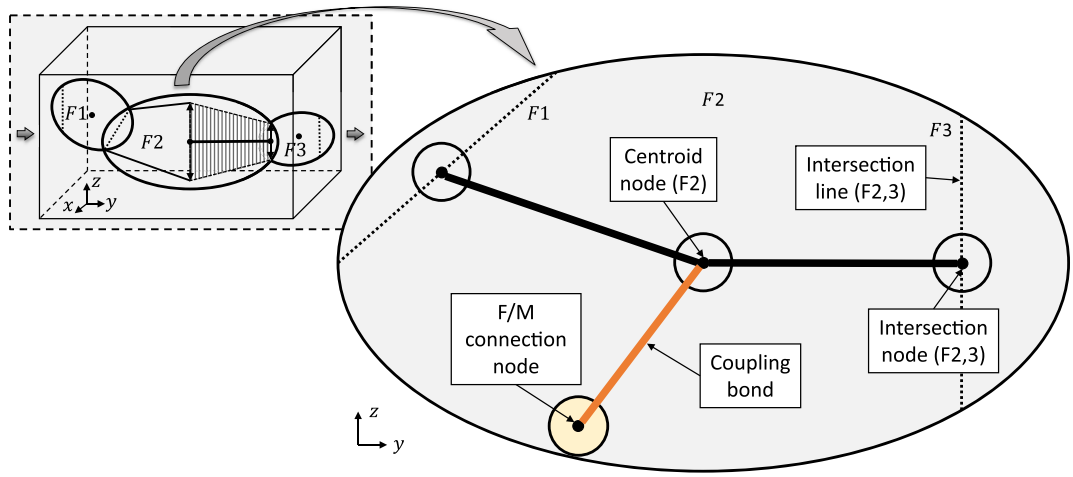

Figure 6. Illustration of the coupling bonds that combines the two networks in 3D, where the orange bond is the coupling bond that communicates the flow between fracture F2 and pore matrix (not visualized here) through the F/M connection node (the light gold node).

construction of fracture pipe network from two perspectives (Wang et al., 2022). First, a new formulation was introduced to assign conductance to the pipe elements and second, the correct topology of the network is ensured. In the current study, we directly adopt the same method to develop fracture pipe network from discrete fractures for 3D case (Wang et al., 2022). The main difference between the current study and the recent published paper is that the former considered both pore matrix and fractures while the latter only dealt with fractures.

In brief, the approach to construct a fracture pipe network is called centroid and intersection line method (CIM). Figure 5 shows an illustration of a simple fracture pipe network of three connected ellipses fractures. A pipe element is built between the centroid point of each fracture and the midpoint of the intersection line or trace. Each pipe is further divided into two node elements connected by one bond element. For more information of the improved fracture pipe network model, please refers to our recent paper (Wang et al., 2022).

2.1.4. Coupling the Two Networks

After the pore network and fracture pipe network are extracted, they are coupled together by the F/M connections. Similar to the extraction of the networks, there is slight difference between coupling 2D and 3D networks. For the 2D case, since F/M connection nodes locate between the boundary nodes and branch nodes, bonds are added between them. That means, previous fracture pipe is broken to add the F/M connection nodes to avoid the possibility of the overlap between the pipe elements, which could lead to extra pressure loss during simulation.

However, in 3D case, as shown in Figure 6, we introduce the "coupling bonds" to join the above two networks. The orange coupling bond is connected between the "F/M connection node" and fracture centroid node. The properties assigned to coupling bonds are the harmonic mean of the two connected nodes, for example, the inscribed radius of the coupling bond is the harmonic mean of the radius of the two nodes. As we can see, the fracture in 2D is split into several segments, which is an implicit representation of fractures and the treatment is similar to that of traditional pore network method. However, the fracture in 3D is represented by equivalent fracture pipes, which is a true coupling network. Coupling bonds in 3D communicate fluid transfer between a fracture and pore matrix, but they do not affect the number of fracture pipes constructed. Fracture pipes are determined by the connections between fractures.

After the coupling network is built, some post processes are implemented on all pore elements. The details of post processes can be referred from our recent work (Wang et al., 2022). The main reason for this step is to ensure the correctness of the topology of the coupling network. Here a brief introduction of some processes is presented, for example, two nodes are merged together if the Euclidean distance between them is smaller than the maximal radius of the two nodes. Bonds are deleted if they connect with the same node. But if they are from different fractures, they are merged and superposition principle is used to assign the conductance, that is, adding their conductance together.

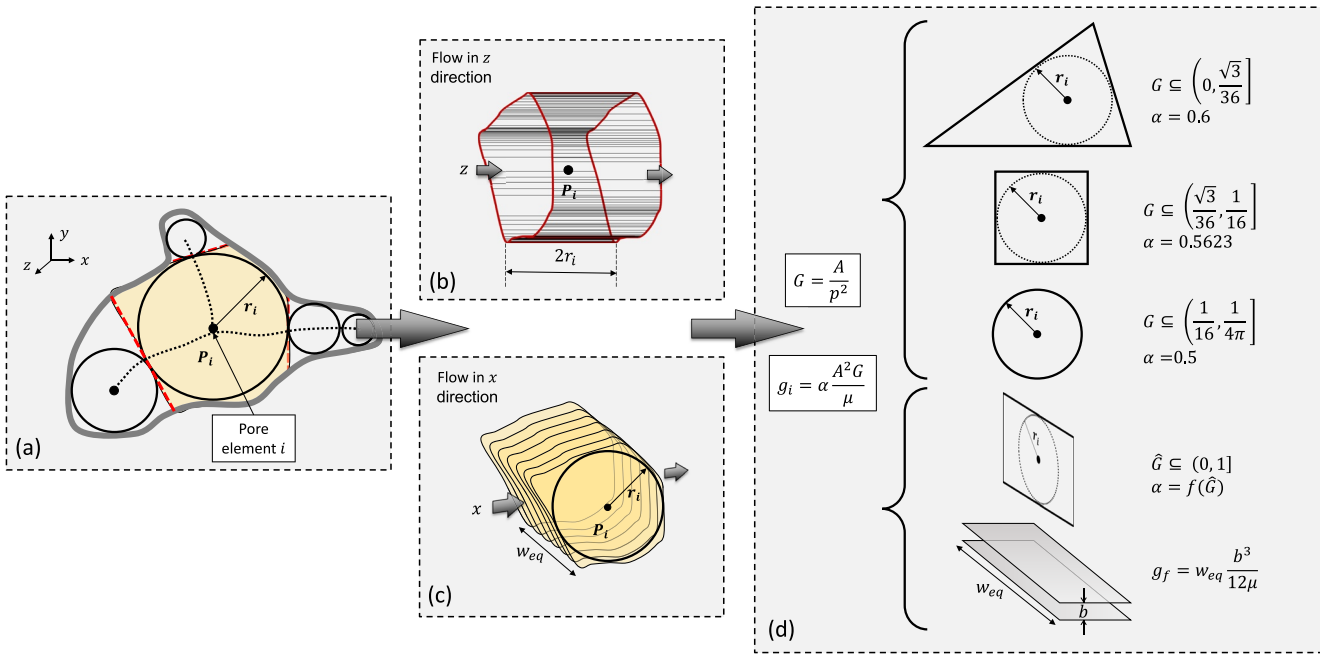

Figure 7. Illustration of the procedures to assign conductance for a pore element in pore network method. (a) A segmented pore element *i*, where the radius r_i and pressure *P* are displayed, and the cross-sectional area *A* and perimeter *p* are determined from the orange shaded zone. (b) The flow duct of element *i* assuming the fluid flow direction is along *Z* axis, noting that the real cross section along *Z* axis is unknown whereas the displayed is just a simplification. (c) The flow duct assuming flow direction is along *X* direction, where a sequence of 2D images is assumed to create a pseudo 3D image. (d) The real cross section is converted to a regular shape so that an appropriate conductance equation is chosen. Shape factor *G* is used to distinguish each pore element. Triangular, square and circle are the three basic shapes assumed in traditional pore network method, whereas rectangular shape and parallel plate model are proposed for the pseudo 3D image and fracture element. In addition, conductance equations can be found in Table 1.

2.1.5. Conductance Assignment

One pore element parameter is of great importance when computing fluid flow properties, that is the conductance.

Figure 7 elucidates the procedures used by the traditional and the new pore network method to assign hydraulic conductance for a pore element. First, pore space is partitioned so that the cross-sectional area *A* and perimeter *p* of a pore element are determined, and the corresponding shape factor, *G*, is defined as:

$$G = \frac{A}{p^2} \tag{1}$$

is used to distinguish these pore elements.

In the coupled network, the pore elements are divided into two categories, depending on whether they are related to fractures or not. Pore elements in the pore matrix, F/M connections and coupling bonds adopt traditional strategy to be assigned with conductance, that is, determined by shape factor (Patzek & Kristensen, 2001). Three different shapes are used viz: circular, square and triangular. This work was done by Patzek and Kristensen (2001), who derived the conductance equations from Stokes equation for different cross-sectional shapes. The shape factors for equilateral triangular, square and circle are $\sqrt{3}/36$, $1/16$ and $1/4\pi$, respectively. The corresponding conductance equations can be found in Table 1.

Fracture pipe elements have a different analytical solution of Stokes equation and therefore they are treated separately. The cubic law equation is adopted to assign conductance for fracture elements, as shown in Table 1 (Sarkar et al., 2004; Witherspoon et al., 1980).

In addition, we introduce the rectangular shape, which has been illustrated in our past paper, but we want to provide a brief summary here for completeness (Wang et al., 2020). First, a rectangular shape cross section is used as a special case when several identical 2D images are stacked together to create the pseudo 3D volume. The

Table 1
The Hydraulic Conductance Equations Used to Assign to the Pore Elements in the Coupling Network, Where g Is Conductance, A Is Cross Sectional Area, G and $\hat{G}$ Are Shape Factor, b Is Fracture Aperture, w_{eq} Is Equivalent Fracture Width

Equivalent shape	Hydraulic conductance	Shape factor range
Triangular	$g = 0.6 \cdot \frac{A^2 G}{\mu}$	$G \subseteq \left(0, \frac{\sqrt{3}}{36}\right]$
Square	$g = 0.5623 \cdot \frac{A^2 G}{\mu}$	$G \subseteq \left(\frac{\sqrt{3}}{36}, \frac{1}{16}\right]$
Circular	$g = 0.5 \cdot \frac{A^2 G}{\mu}$	$G \subseteq \left(\frac{1}{16}, \frac{1}{4\pi}\right]$
Fracture pipe	$g_f = w_{eq} \cdot \frac{b^3}{12\mu}$	-
Rectangular	$g = 0.5623 \cdot \frac{A^2}{16\mu}\left(0.3214\hat{G}^3 + 0.063\hat{G}^2 + 0.6109\hat{G}\right)$	$\hat{G} \subseteq (0, 1]$

Note. The shape factor of a pore element is calculated first, then the equivalent shape is found to calculate the hydraulic conductance.

reason is that we use Palabos with a 3D image to perform Lattice Boltzmann method (LBM) simulation to benchmark our network model (Latt et al., 2020) and accordingly, the pore elements in the network method should also be 3D elements. When using the pseudo 3D volume and assuming the fluid flow direction is parallel to the 2D image plane that is, in X direction, the cross sectional shape of pore element is rectangular. Therefore, the conductance for rectangular shape is adopted for the pseudo 3D scenario. It should be noted that only 2D cases use the conductance of rectangular shape, while pore elements in 3D cases apply more realistic cross sections and equivalent shapes to compute the conductance. $\hat{G}$ is first calculated from $\hat{G} = 16G$ (Patzek & Silin, 2001), and conductance can be calculated consequently from Table 1. The difference in the conductance between rectangular shape and cubic law is negligible when the width to aperture ratio is larger than 50. The details of this conclusion are discussed in Text S1 in Supporting Information S1.

2.2. Fluid Flow Simulation

This section introduces the assumptions used in the fluid flow simulation for both network method and lattice Boltzmann method. The governing equations are Stokes Equation 2:

$$\mu \nabla^2 \vec{u} - \nabla P = 0 \tag{2}$$

where μ is the fluid dynamic viscosity, $\vec{u}$ is the fluid velocity, P is the pressure.

In this work, we consider the single phase flow and the model is fully saturated with water. Typical values of water density and viscosity are used. Flow is incompressible laminar flow and on steady state. Constant pressure boundary conditions are applied to the model inlet and outlet, and the other faces of the model are no-flow boundaries.

2.2.1. Network Method

Fluid flow can be simulated directly in the fracture matrix pore network. First step is to calculate the geometric properties of all elements, including the inscribed radius, cross sectional area, shape factor, etc. Fluid flow for each element, which in fact is an analytical solution of the Stoke's equation, is incorporated via the conductance as discussed in the above section.

The network method has the simplest calculation unit of two nodes connected with one bond (Valvatne & Blunt, 2004). Fluid pressures are defined at the center of the node elements and pressure drop occurs across bonds between the connected nodes. The Hagien-Poiseuille law is used to calculate the flow rate, which is the analytical solution of Stokes equation for flow in a cylindrical pipe. Flow rate Q_{ij} between two nodes is given by:

$$Q_{ij} = \frac{g_{ij}}{L_{ij}}\left(P_i - P_j\right) \tag{3}$$

where g_{ij} is the harmonic mean conductance between two node elements i, j given by:

$$g_{ij} = \frac{L_{ij}}{\frac{L_i}{g_i} + \frac{L_j}{g_j} + \frac{L_b}{g_b}} \tag{4}$$

and the bond b has length L_b and conductance g_b.

Mass conservation is imposed for each node element i:

$$\sum_{j}^{N_i} Q_{ij} = 0 \tag{5}$$

where j runs over all the bond elements connecting to the node element i. Combining Equations 3 and 5, a linear set of equations can be defined and solved for the node pressures. The number of equations and the number of unknowns is equal to the number of node elements. The linear equations are solved using the algebraic solver in OpenCV (Bradski, 2000).

With the pressure known at the centre of each node element, the total flow rate Q_t is calculated at the inlet and outlet, and the absolute permeability k of the network is found from Darcy's law:

$$k = \frac{Q_t \mu L}{A \Delta P} \tag{6}$$

where A and L are the cross sectional area and length of the studied model.

2.2.2. Lattice Boltzann Method (LBM)

LBM simulations were performed in Palabos, an open-source computational fluid dynamics (CFD) solver based on the C++ (Latt et al., 2020). The D3Q19 discrete velocity scheme and the multiple-relaxation-time models (MRT) were used for the LBM simulations. The initial conditions are zero fluid velocity and a constant pressure gradient in the principal flow direction. Bounce-back boundary conditions are applied at the solid walls and constant pressures are applied at the inlet and outlet. The pressure difference is set as 0.0001 in lattice unit. The typical value of collision operator omega is set as 1.0 and kinematic viscosity is 0.16667. In all cases the simulation converged to a steady state in less than 10,000 iterations.

3. Results and Discussions

In this section, the new method is first benchmarked by LBM simulations for both 2D and 3D cases. Then, results of pore network extracted from fractured porous media by maximal ball method and imagenet is compared to our coupled network (FM-PNM). Rock samples from a North Sea sandstone reservoir are used to justify the FM-PNM, which aims to demonstrate the versatility of our new model to deal with complex pore structures. In addition, the influence of pore matrix and discrete fractures on the fractured porous media is analyzed and discussed. The topological properties between pore matrix and fractured porous media are studied. Finally, the pros and cons of the new method are discussed.

3.1. Benchmarkings of the FM-PNM

3.1.1. 2D Test Cases

As shown in Figure 8a, two test cases are used to benchmark the 2D FM-PNM. They have the same pore matrix, which is an artificial porous medium. Image resolution is 1μm/voxel, and image size is 800 by 800 pixels. Two synthetic DFNs are generated: model M1F1 has 2 fractures while model M1F2 has 8 fractures. Fractures are integrated into the pore matrix to create the fractured porous media. FM-PNM is used to build the coupled network and they are shown in Figure 8b. The close packed circles are used to quantify pore matrix. Fracture is segmented into pieces of pipes by boundary nodes, F/M connection nodes and branch nodes, where bond elements are connected between them. Figure 8c shows the velocity streamline simulated by LBM.

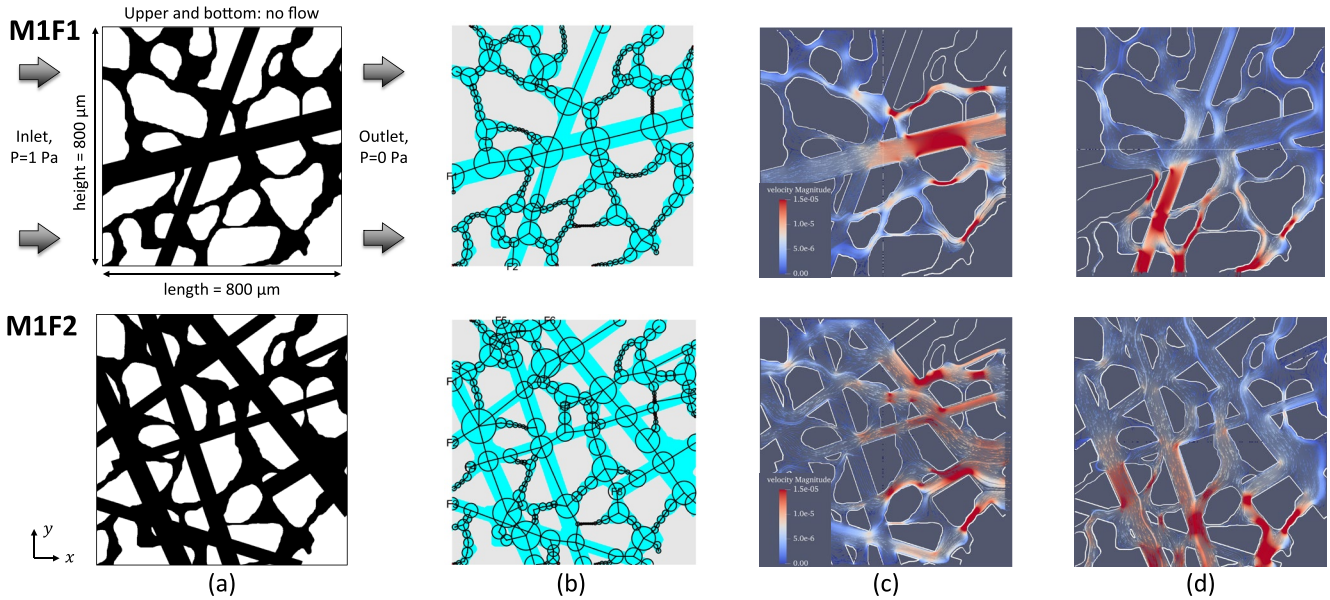

Figure 8. Two test cases are used to benchmark the FM-PNM in 2D. (a) The fractured porous media. (b) Illustration of the coupled network, where circles are the node elements used to quantify the pore structure, and black lines are the bonds connecting nodes. Velocity streamline simulated by lattice Boltzmann method in (c) *X* and (d) *Y* direction, where velocity streamline is tangential to the velocity direction and is used to visualize the motion of a flow. The color represents the velocity magnitude, and red color shows faster flow rate than blue one.

Since LBM simulation requires 3D porous medium, we used 10 identical 2D images to create the pseudo 3D volume. Fluid flow is conducted parallel to the 2D image plane rather than perpendicular to it. In addition, to make sure the network results are comparable to the LBM results, the conductance assigned to 2D pore elements uses the rectangular shape cross sectional area equation as shown in Table 1.

Table 2 shows the permeability calculated by FM-PNM and LBM for 2D test cases. The percentage of deviation is calculated from:

$$\text{deviation} = \frac{k_{\text{net}} - k_{\text{LBM}}}{k_{\text{LBM}}} \times 100\% \tag{7}$$

Comparing the results of FM-PNM and LBM, we note that the range of deviations are between −5.1% and 17.41%. In general, the agreements between these two methods are good. Large discrepancy occurs for the model M1F1 in the *Y* direction. The permeability deviations for the model M1 (pore network only model) and F1 (fracture network only model) in *X* and *Y* direction are shown in Table 3. We can see that the large deviation occurs in the *Y* direction for model M1, which is 15.29% compared to the 5.21% in the *X* direction. The velocity streamline profiles for matrix only (M1) are plotted in Figure 9. We can see that the model M1 has more tiny throats in the *Y* direction than the *X* direction. LBM is a lattice based method, in general, the finer the mesh is, the more accurate the results are. It has large numerical errors in small pore throats, which explains the large discrepancy between the pore network method and LBM for the model M1 in the *Y* direction. The comparisons between pore matrix only, fractures only and coupled fracture and pore matrix will be further discussed later in Section 3.4.

Table 2
Permeabilities for the Two Examples Calculated From Fracture Matrix Pore Network Model and LBM Respectively

	k_x (mD)			k_y (mD)		
Model name	FM-PNM	LBM	Deviation (%)	FM-PNM	LBM	Deviation (%)
M1F1	1476.29	1555.66	−5.10	1597.6	1360.68	17.41
M1F2	2411.64	2236.22	7.84	2362.87	2449.64	−3.54

Table 3
Permeabilities of Model M1 and F1 Calculated by Pore Network Method and LBM

Model name	k_x (mD)			k_y (mD)		
	Network	LBM	Deviation (%)	Network	LBM	Deviation (%)
M1	749.59	712.48	5.21	915.45	794.05	15.29
F1	690.77	752.07	−8.15	427.15	455.63	−6.25

3.1.2. 3D Test Cases

In addition to the demonstration example shown in the section of methodology, another set of synthetic discrete fractures are proposed and integrated with Berea sandstone sample to create the fractured porous medium. We name these two test cases S9F1 and S9F2. Figure 10 (a) shows the two test cases. Model S9F1 has 5 regular fractures while model S9F2 has 8 fractures. The properties of the discrete fractures are saved in the data repository and links are provided in the Data Availability Statement section below. These two models are used to verify the accuracy of the FM-PNM in 3D network. A laptop computer is used to conduct lattice Boltzmann simulation, the memory (32 GB RAM) is not enough to handle the image size as larger as 300^3 voxels, so we use 100^3 voxels of images instead. The second column in Figure 10 shows the coupled network by different colors. Red and orange colors represent the fracture pipe network which is equivalent to the discrete fractures on the left, while blue colors are the network elements of pore matrix. The third column of Figure 10 shows the velocity profile simulated by LBM.

Table 4 reports the permeability calculated by FM-PNM and LBM in *X*, *Y* and *Z* directions, as well as the deviations with LBM. There is good agreement between the newly developed FM-PNM method and LBM, which demonstrates that FM-PNM can reasonably calculate permeability from fractured porous media for 3D samples. In addition, on a personal laptop computer (Intel Core i7 CPU, 32GB RAM), the average total computation time (model construction and permeability calculation) for the FM-PNM is around 50 s, which is much faster than that of the corresponding LBM solution with an average of 500 s.

3.2. Comparisons Between FM-PNM and PNM

Traditional pore network methods are capable of extracting pore networks from porous media, for example, the maximal ball method, medial axis method, watershed method and imagenet tool. They have been justified by a large number of different porous media (Dong & Blunt, 2009; Gostick, 2017; Jiang et al., 2007; Rabbani et al., 2014; Scott, 2020). However, how do pore network methods perform in porous media with fractures? Here, maximal ball method and imagenet tool are employed to extract a pore network directly from fractured porous media, just as that shown in Figure 10 (Bultreys et al., 2018; Dong & Blunt, 2009; Raeini et al., 2017; Scott, 2020). The results are compared to that from the coupled network FM-PNM considered in the current study. Table 4 shows the results computed from maximal ball method and imagenet. Combined with the results in Table 4, the permeabilities calculated by these three methods as well as LBM are plotted in Figure 11. It is clear that the results from both of maximal ball method and imagenet agree poorly with LBM while the agreement between FM-PNM and LBM is good. Therefore, pore network methods perform well in matrix only porous media but have large deviations in fractured porous media. One reason is that the maximal ball algorithm and imagenet are developed for porous media without fractures, so that the extracted network cannot represent fractures properly. More importantly, pore elements in fractures should be assigned a conductance which should be different from that of traditional pore bodies and throats.

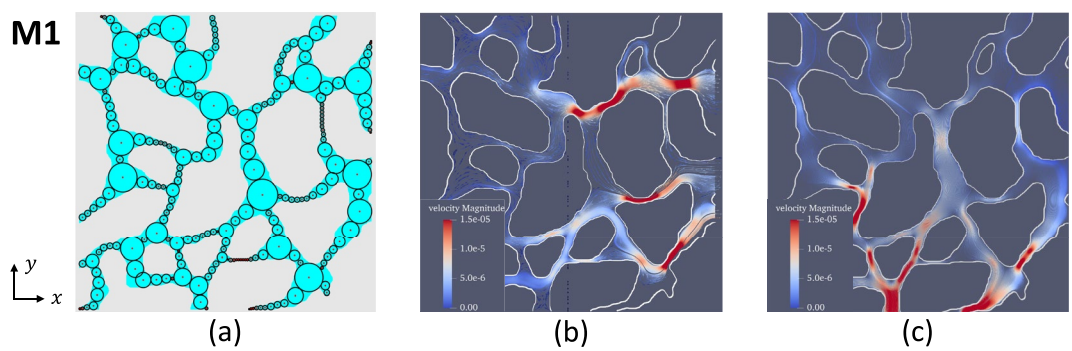

Figure 9. (a) Illustration of pore matrix model M1. (b) Pore network model. Velocity streamline profiles simulated by Lattice Boltzann method in (b) *X* and (c) *Y* direction.

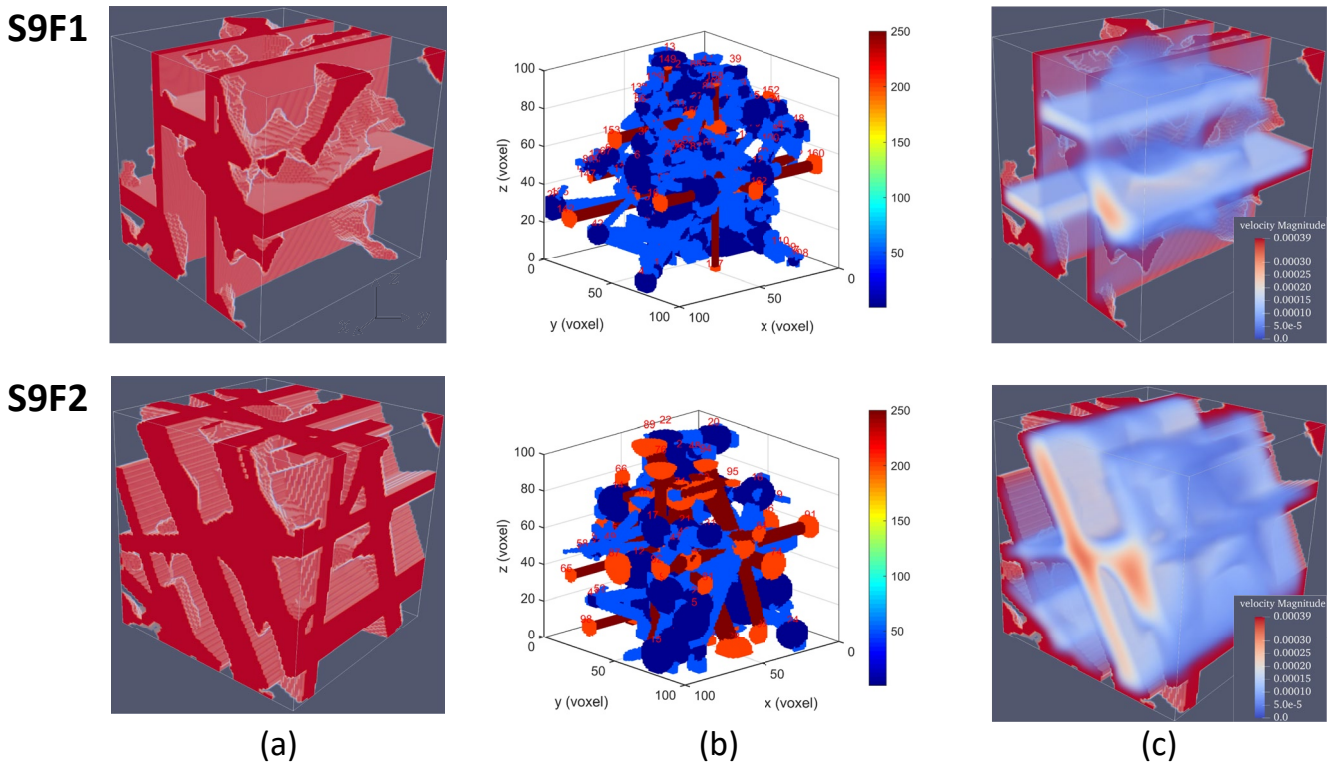

Figure 10. Two test cases are used to justify the FM-PNM. (a) The fractured porous media, artificial fractures are integrated into pore matrix that is from Berea sandstone sample S9, the image size is 100^3 voxels, and image resolution is 1μm/voxel, (b) illustration of the coupled pore network and fracture pipe network, where red and orange colors represent fracture pipe network elements and blue colors represent pore network elements, (c) velocity profile simulated by Lattice Boltzmann method in *X* direction.

3.3. Results of Guillemot A Field Samples

In this section, the samples from Guillemot A field are used as the pore matrix to create fractured porous media. Guillemot A field is a North Sea sandstone reservoir which has undergone long diagenetic history and accordingly

Table 4
Permeabilities Calculated From the FM-PNM Method, the "Imagenet" Tool and the Maximal Ball Method (MB) Compared to LBM for the Two Fractured Porous Media S9F1 and S9F2

	k_x (mD)		k_y (mD)		k_z (mD)	
Model name	Network	LBM	Network	LBM	Network	LBM
S9F1 (FM-PNM)	2340.16	2485.89	1276.83	1299.25	1120.84	950.25
Deviation (%)	−5.86	-	−1.73	-	17.95	-
S9F2 (FM-PNM)	10302.9	10880.2	8060.16	7643.46	11251.7	11079.4
Deviation (%)	−5.31	-	5.45	-	1.56	-
S9F1 (imagenet)	2600.8	2485.89	818.7	1299.25	1836.4	950.25
Deviation (%)	4.62	-	−36.94	-	93.25	-
S9F2 (imagenet)	20272	10880.2	13786	7643.46	13836	11079.4
Deviation (%)	86.32	-	80.36	-	24.88	-
S9F1 (MB)	2092.39	2485.89	1610.53	1299.25	655.849	950.25
Deviation (%)	−15.86	-	23.96	-	−30.98	-
S9F2 (MB)	7643.69	10880.2	7787.45	7643.46	8056.26	11079.4
Deviation (%)	−29.75	-	1.88	-	−27.29	-

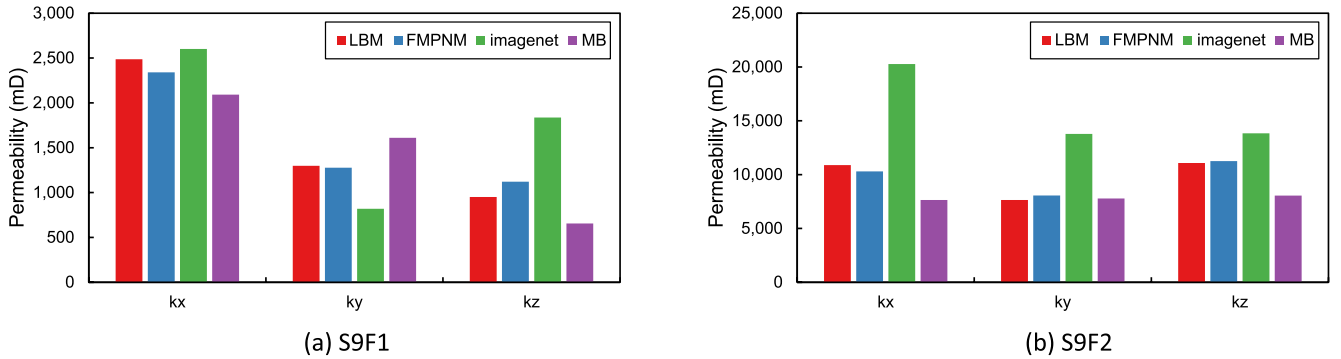

Figure 11. Permeabilities of the three network methods, FM-PNM, imagenet and maximal ball, compared with Lattice Boltzann method for the 3D fractured porous media S9F1 and S9F2.

has a complex pore structure. Two samples with distinct pore structures, plug 44 and 130, are used here and discrete fractures are integrated to construct fractured porous media. The pore matrix, DFN and fractured porous media of these two samples are shown in Figure 12. The measured absolute permeability (air permeability) for plug 44 and 130 are 557 mD and 23 mD respectively. From visual inspection, we can see plug 44 and 130 have more complex and heterogeneous pore structures than Berea sandstone sample. Cumulative pore size distribution curves are plotted for the pore matrix only for plug 44, 130 and Berea sandstone, shown in Figure 13. It shows that pore size of plug 44 and 130 are smaller than Berea sandstone sample, and pore size of plug 130 is the smallest.

Similarly, FM-PNM is used to extract the coupled network from the fractured porous media of Guillemot A field. Permeability is calculated and compared with LBM. The results are reported in Table 5 and shown in Figure 14. It can be concluded that FM-PNM provides a reasonably good permeability for samples from Guillemot A field.

3.4. Comparisons Between Matrix, Fractures and Coupled Fracture and Pore Matrix

In this section, results from pore matrix only, fractures only, and coupled fracture and pore matrix are presented and analyzed. Similarly, it is divided into two parts in terms of 2D and 3D separately.

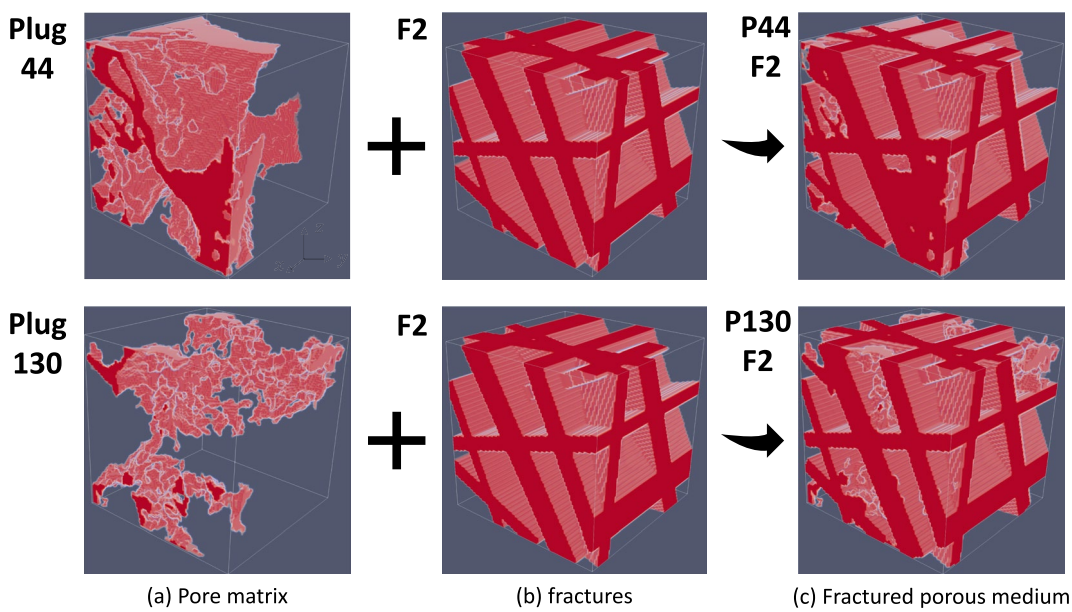

Figure 12. Porous media of plug 44 and 130 are from Guillemot A field, which are used to create fractured porous media. The image size is 100^3 voxels, and image resolution is 1μm/voxel.

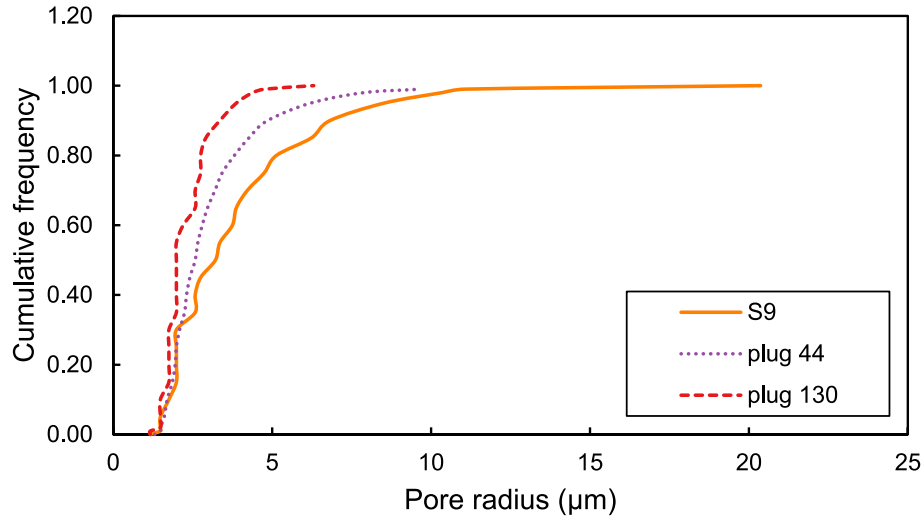

Figure 13. Cumulative pore size distribution curves for pore matrix of Berea sandstone sample, plug 44 and 130.

3.4.1. 2D Scenarios

The same samples presented in Figure 8a are used for 2D cases. Our new pore quantification tool is used to extract the pore network in the pore matrix (Wang et al., 2020) while for the DFN, boundary nodes and branch nodes are used to construct the fracture pipe network. These networks are shown in the first row of Figure 15, which is the supplementary network for the coupled network of FM-PNM 2D as shown in Figure 8. In addition, LBM is used to justify all of the network permeability results. Figure 15 shows the velocity profile simulated by LBM. Table 6 reports the results of permeabilities.

Permeabilities calculated from network for pore matrix only and discrete fractures only show reasonably good agreement with LBM. This on the one hand demonstrates the accuracy of our pore network extraction algorithm and the fracture pipe network method in 2D (Wang et al., 2020). On the other hand, it demonstrates the network method is a good representation of porous media and an efficient method of fluid flow simulation. Additional information of the comparisons between matrix, fractures and F/M are put in Text S2 in Supporting Information S1.

3.4.2. 3D Scenarios

The samples studied are the same as those shown in Figure 10, that is, the test cases S9F1 and S9F2. The imagenet tool is used to extract pore network (PNM) from pore matrix only (Scott, 2020), improved fracture pipe network model (FPNM) is used for the DFN (Wang et al., 2022), and FM-PNM is used for the fractured porous media.

Since the pore network method, improved fracture pipe network and the new coupling network have been justified, only the results from network are reported and shown in Table 7. Permeability ratios between fractured porous media and the summation of matrix and fractures are also presented.

Table 5
Permeabilities of Guillemot Field Samples Integrating With Synthetic Fractures Calculated From FM-PNM and LBM Respectively

	k_x (mD)		k_y (mD)		k_z (mD)	
Sample name	FM-PNM	LBM	FM-PNM	LBM	FM-PNM	LBM
plug 44 + F2	12139.7	13025.1	10438.6	10864.2	15034.1	14765.5
Deviation (%)	−6.80	-	−3.92	-	1.82	-
Plug 130 + F2	9154.04	8670.61	8293.88	6727.57	9904.1	9310.32
Deviation (%)	5.58	-	23.28	-	6.38	-

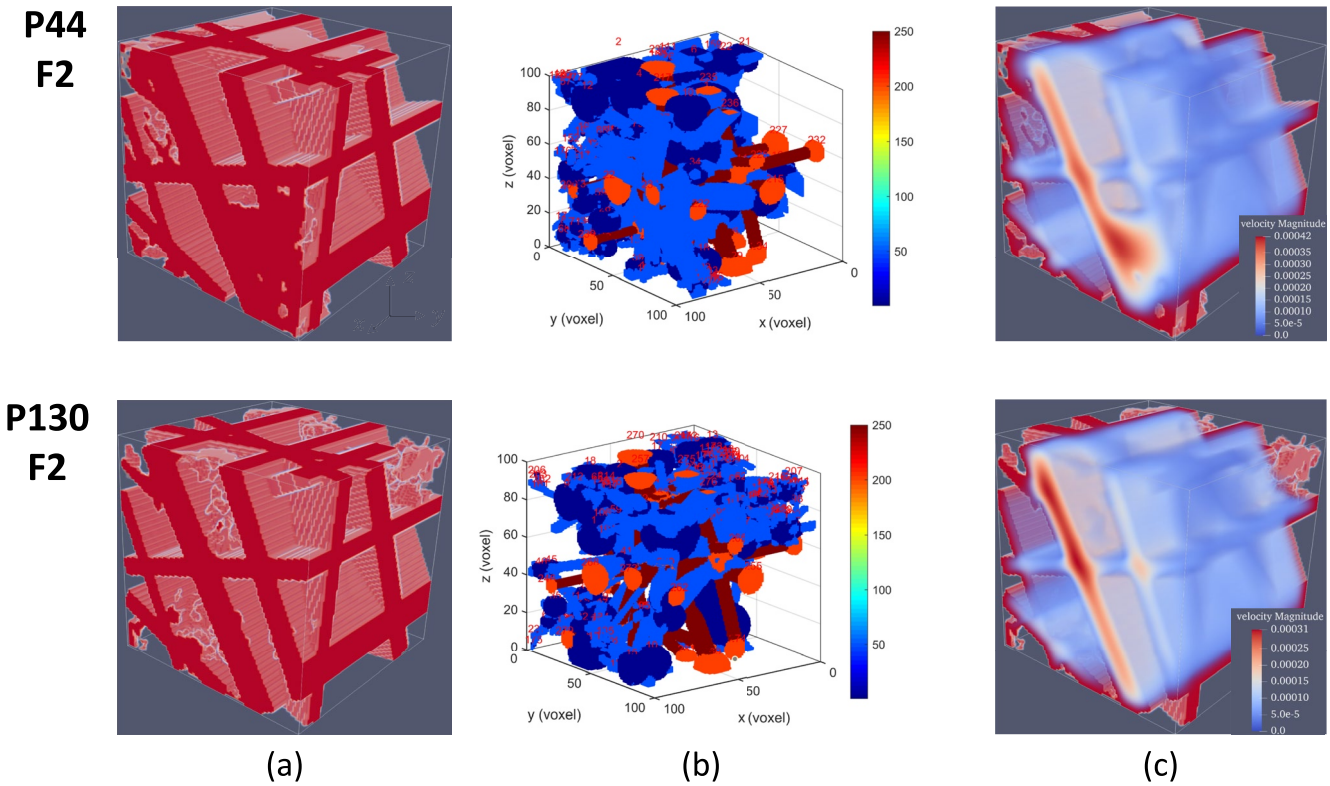

Figure 14. Results for the porous media from Guillemot A field. (a) The fractured porous media, (b) coupled pore network and fracture pipe network, where red and orange colors represent pipe network elements and blue colors represent pore network element, (c) velocity profile simulated by lattice Boltzmann method in *X* direction.

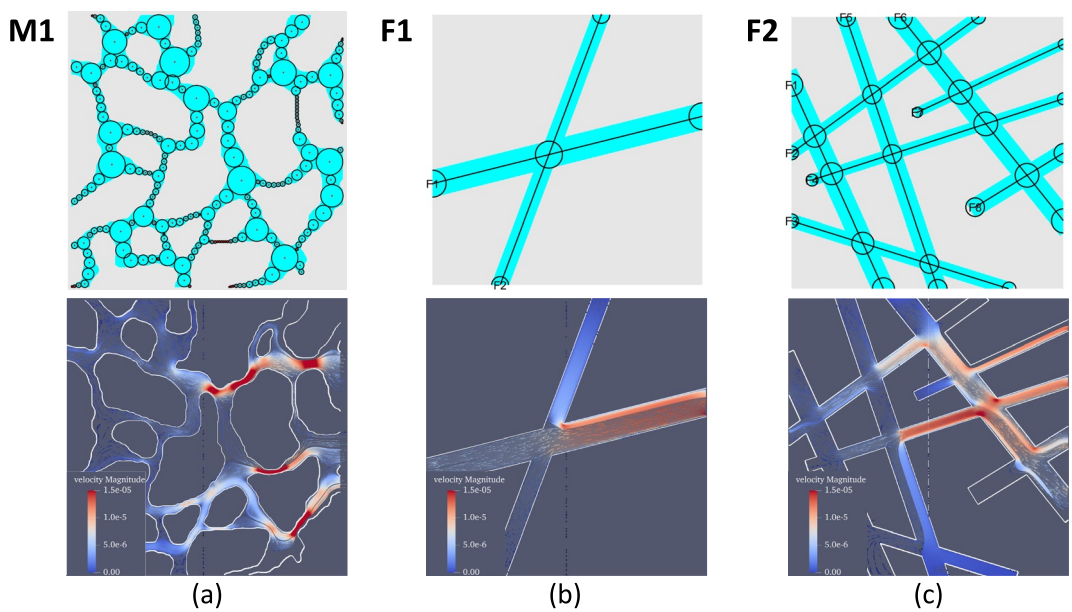

Figure 15. Illustration of the pore matrix and discrete fractures used in 2D case. (a) Pore matrix, (b) discrete fracture model 1 has 2 fractures, (c) fracture model 2 has 8 fractures. The first row shows the porous media in blue color as well as the pore network and second row shows the velocity profile simulated by Lattice Boltzann method in *X* direction.

Table 6
Permeabilities of Pore Matrix and Discrete Fractures for 2D Cases, and Permeability Ratio Between Fractured Porous Media and the Summation of Matrix and Fractures

	k_x (mD)			k_y (mD)		
Model name	Network	LBM	Deviation (%)	Network	LBM	Deviation (%)
M1	749.59	712.48	5.21	915.45	794.05	15.29
F1	690.77	752.07	−8.15	427.15	455.63	−6.25
F2	809.79	878.16	−7.79	1005.82	1051.95	−4.39

Similar to the 2D case, the permeabilities from fractured porous media are larger than that from pore matrix and fractures separately, and even larger than their permeability summations. The permeability is increased because the fractures used here are all open and enhance the connectivity of the system. The relations between the effective permeability of a fractured porous medium and that from pore matrix and fractures respectively are analyzed. For the case S9F1, permeability of fractured porous media (k_{FM}) is more than twice the arithmetic summation of matrix and fractures ($k_M + k_F$). However, k_{FM} is only about 20% higher than $k_M + k_F$ in the case S9F2. The difference between the S9F1 and S9F2 is that S9F1 has smaller differences of k_F/k_M than those of the S9F2. In the traditional reservoir simulations, dual porosity and dual permeability model is usually employed for fractured porous media, which requires matrix and fractures properties within a grid block be specified initially (Bear, 1993). Matrix permeability is generally obtained from experiments, while fracture permeability is determined using the parallel plate analogy and cubic law (Choi et al., 1997). Our research shows that the smaller the difference between k_F and k_M, the larger difference between k_{FM} and $k_M + k_F$.

The fracture density of the two models are calculated. For 3D case, one definition of fracture density is the cumulative fracture area in a unit volume:

$$\rho_f = \frac{\sum A_f}{V} \tag{8}$$

Fracture density for test cases S9F1 and S9F2 are 0.0299 m^{-1} and 0.0724 m^{-1} respectively. Permeability ratios between fracture and pore matrix are shown in Table 7. Case S9F2 has higher fracture density than S9F1 as well as larger fracture and matrix permeability ratio. This shows that the fractures in the case S9F2 dominate the overall flow, therefore, k_{FM} of case S9F2 is closer to the fracture permeability. The relationship between fracture density and permeability ratio $k_{FM}/(k_M + k_F)$ is a future research topic. This will potentially show how to assign the correct permeability for fractured porous media based on the analysis of pore matrix and fractures separately, for example, in reservoir simulations.

In addition, the effect of pore matrix on fractured porous media is discussed. However, no general implication can be concluded due to the limitations of test examples used in this paper in terms of the sample's size, representativeness, etc. Readers who are interested in the analysis between the permeability of k_{FM} and k_M can find some discussions in the Text S3 as shown in Supporting Information S1.

Furthermore, the **topological properties** between pore matrix and fractured porous media are analyzed. Figure 16 shows the Euler characteristic and connectivity coefficient curves for the fractured porous media P44F2 and the pore matrix model P44.

Table 7
All Permeabilities Are Calculated Based on Network Model, Where M Stands for Matrix, F Is Fracture, and FM Are Both Matrix and Fractures

	S9F1			S9F2		
Permeability	k_x (mD)	k_y (mD)	k_z (mD)	k_x (mD)	k_y (mD)	k_z (mD)
k_M (mD)	295.11	199.62	64.943	295.11	199.62	64.943
k_F (mD)	862.73	128.734	223.932	7689.73	6435.47	9549.35
k_{FM} (mD)	2340.16	1276.83	1120.84	10302.9	8060.16	11251.7
$k_{FM}/(k_F + k_M)$	2.02	3.89	3.88	1.29	1.21	1.17
k_F/k_M	2.92	0.64	3.45	26.06	32.24	147.04

Note. Imagenet tool is used for pore matrix only (Scott, 2020), fracture pipe network model is used for the DFN, and FM-PNM is used for the fractured porous media.

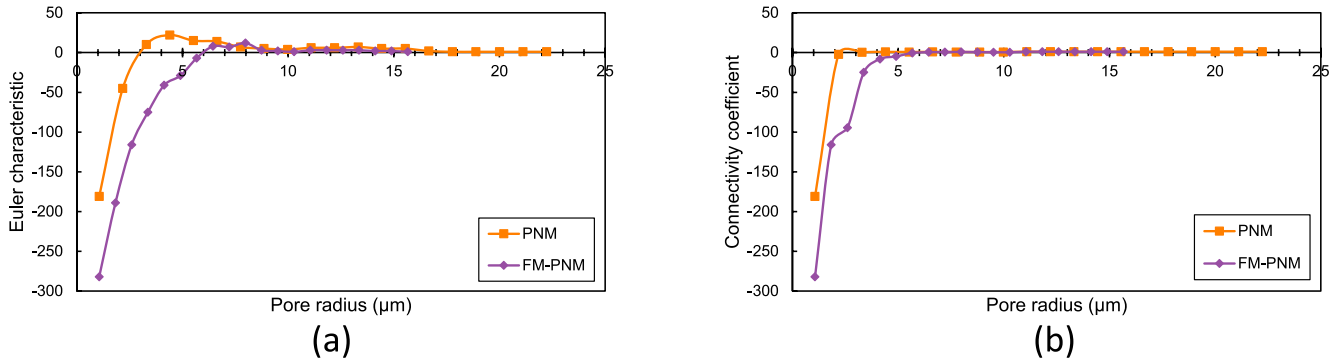

Figure 16. Topological analysis for the fractured porous media P44F2 and pore matrix model P44, (a) the Euler characteristic and (b) connectivity coefficient curves versus pore radius.

The Euler characteristic χ is a parameter used to quantify the topology of the network and is an invariant parameter under continuous deformation of void spaces (M. J. Blunt, 2017; Jiang et al., 2013; Ushizima et al., 2012). For a fully connected pore network, the Euler characteristic is given by:

$$\chi = N_n - N_b \tag{9}$$

In general, the larger the absolute Euler characteristic, the better the connectivity. The Euler characteristic χ can also be calculated from the Betti numbers (M. J. Blunt, 2017):

$$\chi = \beta_0 - \beta_1 \tag{10}$$

where β_0 reflects the number of isolated clusters and β_1 is the number of handles or loops in the network. The smaller the β_0, the better the connectivity. Therefore, a new topology descriptor is introduced to quantify the connectivity of a pore network, which is called the connectivity coefficient, ψ:

$$\psi = \frac{\chi}{\beta_0} \tag{11}$$

It can be seen that the larger the absolute χ is, the better the connectivity is.

The specific connectivity function or intensive Euler characteristic is the relationship between the Euler characteristic and pore radius in a unit volume, which is given as:

$$\chi_V(r) = \frac{N_n(r) - N_b(r)}{V} \tag{12}$$

where $N_n(r)$ is the number of nodes with radius larger than r; $N_b(r)$ is the number of bonds that satisfying two criteria. First, bond radius is larger than the given radius r; second, radius of the two connected nodes should also be larger than the given radius.

The connectivity function is important for single phase and multiphase flow behavior. If $\chi_V(r) < 0$, then the sub-network is connected for radii larger than r and vice versa. The critical radius r_c is found when $\chi_V(r) = 0$, which corresponds to the macroscopic capillary entry pressure (Scott, 2020).

The absolute connectivity coefficient for the model P44F2 is 282, which is 55.8% larger than the model P44 ($\psi = 181$). The fractured porous media has a better connectivity than the pore matrix. The permeabilities of P44F2 (12 139.7 mD) is 16 times larger than the P44 (750.32 mD). It is clear that the connectivity has a significant impact on the permeability.

Figure 17 compares the connectivity coefficient curves of the three fractured porous media, that is, P130F2, S9F2 and P44F2. The P44F2 has the largest critical radius (5.71μm), then the S9F2 (5.67μm) and P130F2 has the smallest critical radius (4.99μm). The permeability also shows the same trend. P44F2 has the largest permeability (12 139.7 mD), followed by S9F2 (10 302.90 mD) and P130F2 has the smallest permeability (9154.04 mD). Therefore, the larger the critical radius is, the larger the permeability is.

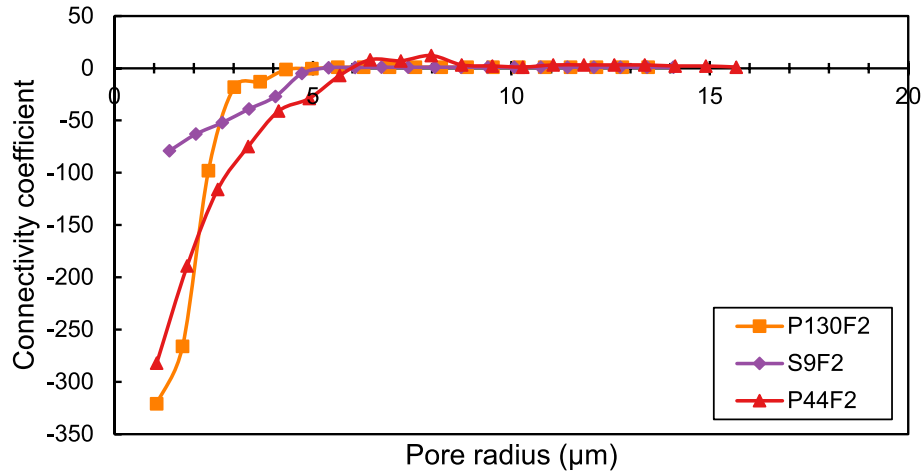

Figure 17. Connectivity coefficient versus pore radius curves for the three samples of fractured porous media.

On the other hand, even though the model P130F2 has the largest absolute connectivity coefficient as shown in Figure 17 (the bottom left endpoint on the curve), its connectivity is not the best. Firstly, the absolute connectivity coefficient of the P130F2 has the fastest declining rate. Secondly, the P130F2 has the smallest critical radius. Based on these two indicators, the model P44F2 has the best connectivity, then is the model S9F2, and the model P130F2 has the worst connectivity.

3.5. Discussions on the FM-PNM

In this section, we discuss the advantages and disadvantages of the FM-PNM method as well as the key for representation of fractured porous media. The components of the method are not new because the ideas of pore network modeling and fracture pipe modeling have been available for many years. But when these two networks are coupled together as presented in the current research, it is possible to determine the permeability for fractured porous media with reasonable agreement with lattice Boltzmann method. This is because FM-PNM can represent the fractured porous media reasonably well.

Like the other network methods, for example, the maximal ball or fracture pipe network method, FM-PNM is easy to be understood. The FM-PNM introduce the F/M connections, so it is capable of studying the transport mechanism between fractures and pore matrix. Most importantly, network based methods are efficient approaches because a network is a hydraulically equivalent representation of the porous medium, which dramatically decreases the computational time and resources of fluid flow simulation in porous media. Therefore, network method is capable of dealing with thousands, or even millions of pore elements simultaneously and can be used on larger scale samples efficiently compared to direct simulations (Aghaei & Piri, 2015; Jiang et al., 2013; Mahmoodlu et al., 2020). Conversely, CFD based methods could accurately simulate fluid flow with finely meshed porous media. But in turn, it limits the application of these methods on millions of pore clusters or large scale samples.

3.5.1. The Limitations of FM-PNM

FM-PNM has limitations, which can be viewed from two perspectives, the representation of pore matrix and fractures. The first limitation is that this method is dependent on pore network method and deviations introduced from pore matrix also affect the FM-PNM. For example, Table 8 shows the permeability calculated from imagenet and LBM for plug 44 and 130 matrix only. Firstly, the imagenet tool performs well for most cases. The absolute average deviation for plug 44 is 16.9%. Large deviation of permeability occurs in the *Y* direction for plug 130 compared with LBM, which is 55.57%, however, the deviation in *X* direction is only 8.79%. In addition, Table 5 shows the results of FM-PNM compared to LBM. The deviation of FM-PNM and LBM for plug 130 is 23.28% in *Y* direction and 5.58% in *X* direction. It demonstrates that the deviations introduced from pore matrix affect the FM-PNM.

However, on the other hand, can LBM always compute accurate results? The answer is it depends. LBM is a numerical method, so it also has numerical errors. It is a lattice based method, in general, the finer the mesh,

Table 8
Imagenet and LBM Are Used to Calculate Permeabilities From Only the Pore Matrix of Plug 44 and 130

	k_x (mD)		k_y (mD)		k_z (mD)	
Model name	Imagenet	LBM	Imagenet	LBM	Imagenet	LBM
Plug 44	750.32	897.851	364.43	458.793	1151.5	1334.36
Deviation (%)	−16.43	-	−20.57	-	−13.70	-
Plug 130	16.197	14.8887	6.6952	15.0696	8.5047	12.0096
Deviation (%)	8.79	-	−55.57	-	−29.18	-

the better the results. Micro-CT images have finite resolution, the pore sizes of some rock samples are small and of similar size as the resolution, in which case uncertainties would occur when using simulations of LBM. The research of Pan et al. (2006) shows that the permeability simulated by LBM is dependent on the image resolution and the numerical error is as large as 10% for the grid resolution of 8 lattices. The average pore size of plug 130 is computed as 2.28μm, which is not much larger than the image resolution 1μm/voxel. Figure 12 shows the pore matrix of plug 130 and 144 and we can see that the plug 130 has more tiny throats than plug 44 based on visual inspection. Quantitatively speaking, the percentage of pores that are smaller than 2μm for plug 130 is 57%, which can be referred in the cumulative pore size distribution curve shown in Figure 13, while that percentage for plug 44 is only 25%. Therefore, large numerical errors would be introduced by LBM in modeling fluid flow in plug 130. This could explain the large discrepancy of permeability calculated between the LBM and the network methods.

The second limitation of FM-PNM is related to discrete fractures. We demonstrate this with an example. The Berea sandstone sample is used as the pore matrix while different number of fractures are integrated, the samples are shown in Figure 18. The deviations of permeability between FM-PNM and LBM are reported in Table 9. The deviation between the pore network and LBM for only pore matrix is around 30%. While the deviation between fracture network and LBM is 4% (average deviations in *Y* direction), which is much smaller than for pore matrix. With the increase of fracture density, the relative deviations of FM-PNM are decreasing. That is because the fracture permeability is higher than pore matrix. When fractures density increase, fractures dominate the flow, so that the deviation introduced from pore matrix is reduced.

In addition, the FM-PNM as implemented in the current study neglects effects of the surface roughness of the fracture on the flow regimes and permeability. It does not consider contacts between fracture surfaces leading to localize closure and reduction in fracture permeability either. In fact, one procedure we presumed that has been done before constructing a FM-PNM is the transformation of a realistic fracture into an equivalent discrete fracture. Fracture pipes are then extracted based on the equivalent DFN. We used idealized and smooth fractures because we focused our current study on the development of the framework for the coupling network of fracture and matrix network. The transformation of real fractures into a DFN can be our next work. There are several

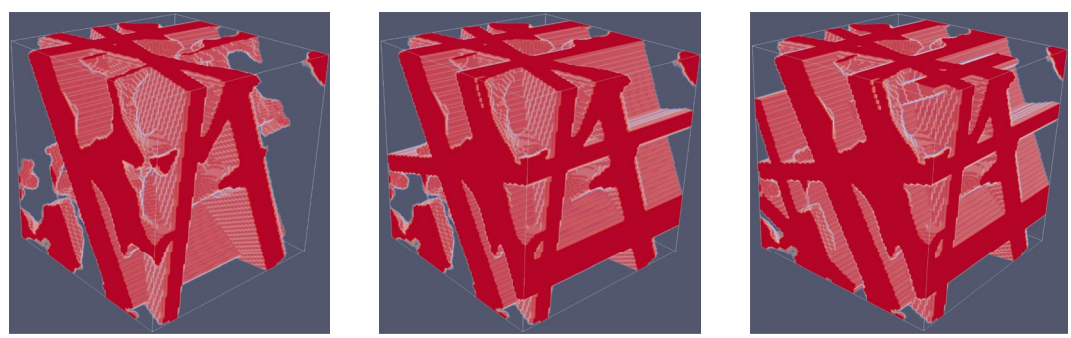

Figure 18. Different number of fractures are integrated into the pore matrix to investigate the effect of numerical errors on calculation, where Berea sandstone sample is used as the pore matrix.

Table 9
Deviations (%) Between Network Method and LBM for the Berea Sandstone Sample With Different Fracture Number, Where M Stands for Matrix, F Is Fracture, and FM Are Both Matrix and Fractures

	Deviation in *Y* direction			Deviation in *Z* direction		
Model name	M	F	FM	M	F	FM
S9	−32.91	-	-	−36.32	-	-
S9 + 3 fractures	−32.91	−4.84	22.82	−36.32	−0.87	44.64
S9 + 5 fractures	−32.91	−5.53	29.61	−36.32	−2.74	29.73
S9 + 8 fractures	−32.91	−1.65	5.45	−36.32	2.58	1.56

Note. Imagenet tool is used for pore matrix only (Scott, 2020), fracture pipe network model is used for the DFN, and FM-PNM is used for the fractured porous media.

roughness models that can be incorporated into a DFN to represent the realistic fractures, for example, the joint roughness coefficient model and fractal dimension model (Crandall et al., 2010; Jing et al., 2017). Jing et al. (2017) proposed a rough-walled DFN model where fractures have stochastic roughness and fracture aperture is a function of the surface roughness. We are currently developing an effective and automated approach to obtain the deterministic DFN that can equivalently represent a real fracture network. Therefore, methodology developed will be extended in the future work to explore the effects of fracture surface roughness and fracture closures on the flow regimes and permeability.

3.5.2. The Key for Representation of Fractured Porous Media

Implicit representation of fractures has the "meshing" process, whereas explicit representation of fractures is through a hydraulically equivalent substitute and involves less "mesh." For example, methods of an implicit representation of a fracture are the CFD based methods. Hughes and Blunt (2001) applied regular square "mesh" over fractures to construct the network, which is also an implicit representation. On the other hand, the explicit representation method is the fracture pipe network method. Although it also divides fracture space into flow subdomains, the number of such domains is much less than that of implicit method. Some published studies show that fractures implicitly represented by a pore network can also have good results (Hughes & Blunt, 2001; Jiang et al., 2017; Karpyn & Piri, 2007; Rabbani et al., 2020). This raises a question about whether fractures should be represented explicitly or implicitly? Or, in what cases is explicit representation more suitable?

Let's go back to our 2D FM-PNM case. A fracture in 2D is equivalent to a one dimensional pipe object, which is the same as pore body and throat in terms of topology. In 2D FM-PNM, a fracture is partitioned into pipe segments which is reasonable to represent the flow features. In fact, the treatment of fractures in 2D FM-PNM is the same as pore elements in matrix and thus is implicit representation. In the case of 3D FM-PNM, where fracture is explicitly represented by the pipe elements. Fractures are treated implicitly in 2D while explicitly in 3D, however, both treatments have the reasonable results. Therefore, we think the key to get good simulation results is that fracture should be represented properly and conductance is assigned reasonably. It is not that important to differentiate whether fractures are represented implicitly or explicitly.

Last but not least, a realistic fracture sample was investigated. Figure 19a shows the micro-CT image of the sample with two intersecting fractures from a carbonate rock reservoir. The distinct features of real world fractures are the curved and rough walls as well as the changing local aperture sizes, and fractures do not always remain open, as the precipitation of minerals inside fractures could seal and close fractures. An equivalent discrete fracture network is extracted manually and integrated into pore matrix sample S9 to construct the fractured porous

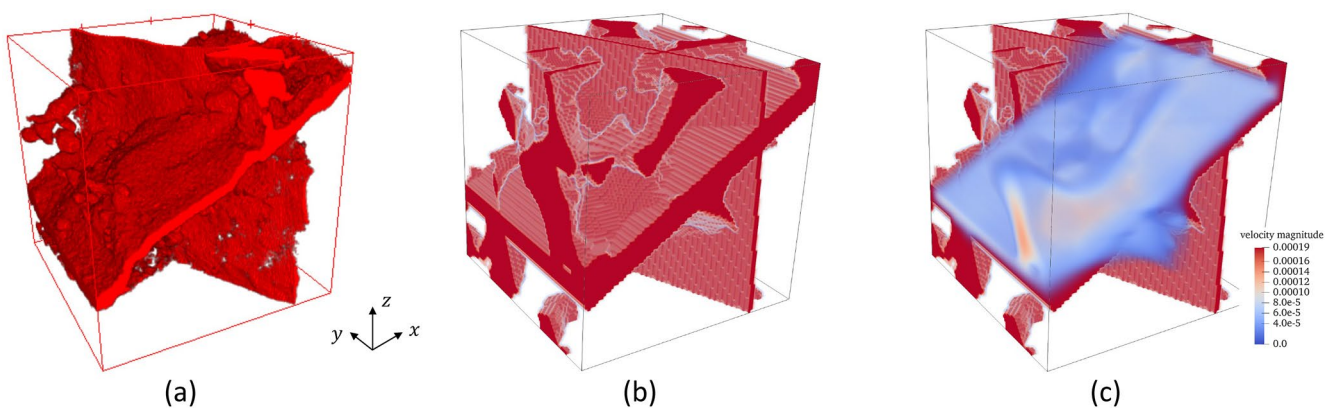

Figure 19. A demonstration of applying the FM-PNM in a real world case. (a) The micro-CT image of a real fractured carbonate sample with two intersecting fractures. The image size is 100^3 voxels and image resolution is 1μm/voxel. (b) An equivalent discrete fracture network was extracted and then integrated into the pore matrix sample S9 to construct the fractured porous medium. (c) The velocity profile as simulated by Lattice Boltzann method in *X* direction.

Table 10
Permeabilities of the Realistic Fractured Sample as Shown in 19(b) That Are Calculated From LBM, the FM-PNM and the Imagenet Tool, Where Deviations Are Compared With the LBM

Method name	k_x (mD)	k_y (mD)	k_z (mD)
LBM	1642.57	1820.23	688.91
FM-PNM	1864.36	1958.19	716.07
Deviation (%)	13.50	7.58	3.94
Imagenet	1496.80	1490.40	1048.80
Deviation (%)	−19.72	−23.89	46.47

medium as shown in Figure 19b. The measurement and extraction of discrete fractures were done by hand using the ImageJ (Schindelin et al., 2012). The FM-PNM is constructed to compute single phase permeabilities, which are presented in Table 10 as well as the permeability simulated by LBM and imagenet tool. It is clear that FM-PNM predicts reasonable results compared to imagenet and proves that fractures should be treated separately.

The essence of fracture pipe network model is to divide fractures into flow subdomains and transform them into equivalent pipes. Flow in ideal DFNs, meaning fractures with regular shape and constant aperture, is identical for each subdomain. Therefore, the flow in fracture can be well represented by pipe elements. A fracture can be connected to many pores in matrix, but it does not mean the fracture should be divided into many pipes. The number of pipes that a 3D fracture is divided depends on the connection of the fracture with *other fractures* rather than with pores in the pore matrix. That means fractures in 3D are divided into few idealized fracture elements rather than a large number of subdomains. These idealized subdomains are extracted from real fractures using specified geometric and topological parameters, such as roughness, range of apertures, shape factor, number of nodes and bonds connected with the fracture. In addition, a fracture pipe network can capture the flow anisotropy even though the DFN is represented by a limited number of pipes. The Text S4 in Supporting Information S1 compares the flow fields computed from the fracture pipe network and the LBM, which demonstrates that the fracture pipe network can capture the flow direction and anisotropy.

4. Conclusions

In this research, we have developed a coupled discrete fracture pore network model (FM-PNM) to represent fractured porous media and efficiently calculate the fluid flow properties. In the coupled network, pore matrix is represented by traditional pore network while discrete fractures are represented by fracture pipe network. The key to build FM-PNM is to find fracture/matrix connection elements so that pore network can be appropriately coupled with fracture pipe network.

The permeability of the FM-PNM is benchmarked by Lattice Boltzmann method for various types of pore matrix as well as different discrete fracture networks. By comparing the network extracted by traditional pore network methods and FM-PNM for fractured porous media, we found that when compared with the LBM, the developed FM-PNM gives a much better prediction of the permeability for fractured porous media than the traditional PNM. The key to good simulation results is that fractures should be represented properly and conductance be assigned reasonably.

Results from pore matrix only, fractures only, and coupled fracture and pore matrix are analyzed and discussed. The permeabilities from fractured porous media are larger than those from pore matrix and fractures separately, and even larger than the summation of their permeabilities. Therefore, the simple arithmetic summation of permeability from pore matrix and fractures cannot represent that of fractured porous media. In addition, the topological properties between pore matrix and fractured porous media are quantified by the connectivity coefficient. Fractured porous media have better connectivity than the pore matrix and the connectivity has a large impact on the permeability.

The network method is very efficient in simulation of fluid flow. But FM-PNM is dependent on the pore network method where the errors introduced from pore matrix affect the FM-PNM. A simple realistic fracture sample is included to demonstrate the application of the FM-PNM in the real world case. Fractures in 3D are divided into few idealized fracture pipe elements rather than a large number of subdomains. Most samples used in this study have small dimensions (<mm) and a small number of pores and synthetic fractures, however, the FM-PNM can be applied to larger scale samples besides the micro-scale ones, for example, core scale fractures or faults. In addition, fractures in the FM-PNM not only have the rectangular shape. Real fractures are extracted and represented using geometric and topological parameters, such as roughness, range of apertures, shape factor, number of nodes and bonds connected with the fracture.

We also want to apply the FM-PNM into more realistic samples, however, the code to extract fractures directly from micro-CT images has not been developed yet. In addition, real rock samples contain both matrix and

fractures, and we don't have codes to differentiate them either. Therefore, we use synthetic test examples to construct fractured samples that real fractures are first converted to DFNs and then embedded into pore matrix.

Nevertheless, FM-PNM method is an evolving and developing method. We plan to extend the applications of this method. For example, fractures with various aperture size distribution will be considered. FM-PNM is based on DFN where the inclusion of fracture roughness can also be considered. In addition, the identification of connections between fractures and pore matrix in current work is important, which plays a role in communicating the transfer of fluid. This should be investigated to study the fluid transfer mechanisms between fractures and pore matrix. Multiphase flow simulation is another important aspect that should be taken into account in the FM-PNM, however, it would be challenging to represent complex fluid occupations in a fracture. One possible approach is that each fracture is discretized into multiple pipes to account for aperture variation within a fracture and to consider multiphase flow, which would be our future work.

Data Availability Statement

The data that support the findings of this research are available in Mendeley data repository (Wang, 2020). All of the parameters of the DFNs (the coordinates, the aperture of the DFNs) used are available in https://data.mendeley.com/datasets/c8r645tj9v/2.

Acknowledgments
C.W. thanks the financial support from China Scholarship Council (CSC) for his Ph.D. study.

References

Aghaei, A., & Piri, M. (2015). Direct pore-to-core up-scaling of displacement processes: Dynamic pore network modeling and experimentation. *Journal of Hydrology*, *522*, 488–509. https://doi.org/10.1016/J.JHYDROL.2015.01.004

Bear, J. (1993). Modeling flow and contaminant transport in fractured rocks. In J. Bear, C.-F. Tsang, & G. de Marsily (Eds.), *Flow and contaminant transport in fractured rock* (pp. 1–37). Academic Press. https://doi.org/10.1016/B978-0-12-083980-3.50005-X

Berre, I., Doster, F., & Keilegavlen, E. (2018). Flow in fractured porous media: A review of conceptual models and discretization approaches. *Transport in Porous Media*, *130*(1), 215–236. https://doi.org/10.1007/s11242-018-1171-6

Blunt, M. J. (2001). Flow in porous media - Pore-network models and multiphase flow. *Current Opinion in Colloid & Interface Science*, *6*(3), 197–207. https://doi.org/10.1016/S1359-0294(01)00084-X

Blunt, M. J. (2017). *Multiphase flow in permeable media: A pore-scale perspective*. Cambridge University Press. https://doi.org/10.1017/9781316145098

Blunt, M. J., Bijeljic, B., Dong, H., Gharbi, O., Iglauer, S., Mostaghimi, P., et al. (2013). Pore-scale imaging and modelling. *Advances in Water Resources*, *51*, 197–216. https://doi.org/10.1016/J.ADVWATRES.2012.03.003

Blunt, M., & Bijeljic, B. (2015). Micro-CT images and networks. Retrieved from https://www.imperial.ac.uk/earth-science/research/research-groups/pore-scale-modelling/micro-ct-images-and-networks/

Bradski, G. (2000). The OpenCV library. *Dr. Dobb's Journal of Software Tools*. Retrieved from https://opencv.org/

Bultreys, T., De Boever, W., & Cnudde, V. (2016). Imaging and image-based fluid transport modeling at the pore scale in geological materials: A practical introduction to the current state-of-the-art. *Earth-Science Reviews*, *155*, 93–128. https://doi.org/10.1016/J.EARSCIREV.2016.02.001

Bultreys, T., Lin, Q., Gao, Y., Raeini, A. Q., AlRatrout, A., Bijeljic, B., & Blunt, M. J. (2018). Validation of model predictions of pore-scale fluid distributions during two-phase flow. *Physical Review E*, *97*(5), 053104. https://doi.org/10.1103/PhysRevE.97.053104

Choi, E. S., Cheema, T., & Islam, M. R. (1997). A new dual-porosity/dual-permeability model with non-Darcian flow through fractures. *Journal of Petroleum Science and Engineering*, *17*(3–4), 331–344. https://doi.org/10.1016/S0920-4105(96)00050-2

Crandall, D., Bromhal, G., & Karpyn, Z. T. (2010). Numerical simulations examining the relationship between wall-roughness and fluid flow in rock fractures. *International Journal of Rock Mechanics and Mining Sciences*, *47*(5), 784–796. https://doi.org/10.1016/J.IJRMMS.2010.03.015

Dershowitz, W., Pointe, P. L., & Doe, T. (2004). Advances in discrete fracture network modeling. In *Proceedings of the US EPA/NGWA fractured rock conference* (pp. 882–894).

Dong, H., & Blunt, M. J. (2009). Pore-network extraction from micro-computerized-tomography images. *Physical Review E*, *80*(3), 1–11. https://doi.org/10.1103/PhysRevE.80.036307

Dunsmuir, J. H., Ferguson, S. R., D'Amico, K., Amico, K. L., & Stokes, J. P. (1991). X-Ray microtomography: A new tool for the characterization of porous media. *SPE Annual Technical Conference and Exhibition*, *61*, 1305–1316. https://doi.org/10.2118/22860-MS

Flannery, B. P., Deckman, H. W., Roberge, W. G., & D'Amico, K. L. (1987). Three-dimensional x-ray microtomography. *Science*, *237*(4821), 1439–1444. Retrieved from https://science.sciencemag.org/content/237/4821/1439

Golf-Racht, T. V. (1996). *Naturally-fractured carbonate reservoirs* (Vol. 44). Elsevier. https://doi.org/10.1016/S0376-7361(96)80029-X

Gostick, J. T. (2017). Versatile and efficient pore network extraction method using marker-based watershed segmentation. *Physical Review E*, *96*(2), 023307. https://doi.org/10.1103/PhysRevE.96.023307

Hughes, R. G., & Blunt, M. J. (2001). Network modeling of multiphase flow in fractures. *Advances in Water Resources*, *24*(3–4), 409–421. https://doi.org/10.1016/S0309-1708(00)00064-6

Jiang, Z., van Dijke, M., Marinus Izaak Jan Geiger, S., Ma, J., Couples, G. D., & Li, X. (2017). Pore network extraction for fractured porous media. *Advances in Water Resources*, *107*, 280–289. https://doi.org/10.1016/J.ADVWATRES.2017.06.025

Jiang, Z., Van Dijke, M., Sorbie, K. S., & Couples, G. D. (2013). Representation of multiscale heterogeneity via multiscale pore networks. *Water Resources Research*, *49*(9), 5437–5449. https://doi.org/10.1002/wrcr.20304

Jiang, Z., Wu, K., Couples, G., Van Dijke, M. I. J., Sorbie, K. S., & Ma, J. (2007). Efficient extraction of networks from three-dimensional porous media. *Water Resources Research*, *43*(12), 1–17. https://doi.org/10.1029/2006WR005780

Jing, Y., Armstrong, R. T., & Mostaghimi, P. (2017). Rough-walled discrete fracture network modelling for coal characterisation. *Fuel*, *191*, 442–453. https://doi.org/10.1016/j.fuel.2016.11.094

Jing, Y., Rabbani, A., Armstrong, R. T., Wang, J., & Mostaghimi, P. (2020). A hybrid fracture-micropore network model for multiphysics gas flow in coal. *Fuel*, *281*, 118687. https://doi.org/10.1016/j.fuel.2020.118687

Karpyn, Z. T., & Piri, M. (2007). Prediction of fluid occupancy in fractures using network modeling and X-ray microtomography. I: Data conditioning and model description. *Physical Review E*, *76*(1), 016315. https://doi.org/10.1103/PhysRevE.76.016315

Latt, J., Malaspinas, O., Kontaxakis, D., Parmigiani, A., Lagrava, D., Brogi, F., et al. (2020). Palabos: Parallel Lattice Boltzmann solver. *Computers & Mathematics With Applications*, *81*, 334–350. https://doi.org/10.1016/j.camwa.2020.03.022

Liu, H., Kang, Q., Leonardi, C. R., Schmieschek, S., Narváez, A., Jones, B. D., et al. (2016). Multiphase Lattice Boltzmann simulations for porous media applications. *Computational Geosciences*, *20*(4), 777–805. https://doi.org/10.1007/s10596-015-9542-3

Mahmoodlu, M. G., Raoof, A., Bultreys, T., Van Stappen, J., & Cnudde, V. (2020). Large-scale pore network and continuum simulations of solute longitudinal dispersivity of a saturated sand column. *Advances in Water Resources*, *144*, 103713. https://doi.org/10.1016/J.ADVWATRES.2020.103713

Meakin, P., & Tartakovsky, A. M. (2009). Modeling and simulation of pore-scale multiphase fluid flow and reactive transport in fractured and porous media. *Reviews of Geophysics*, *47*(3), 1–47. https://doi.org/10.1029/2008RG000263.1.INTRODUCTION

Pan, C., Luo, L. S., & Miller, C. T. (2006). An evaluation of Lattice Boltzmann schemes for porous medium flow simulation. *Computers & Fluids*, *35*(8–9), 898–909. https://doi.org/10.1016/j.compfluid.2005.03.008

Patzek, T., & Kristensen, J. G. (2001). Shape factor correlations of hydraulic conductance in noncircular capillaries II. Two-phase creeping flow. *Journal of Colloid and Interface Science*, *317*(2), 305–317. https://doi.org/10.1006/jcis.2000.7414

Patzek, T., & Silin, D. B. (2001). Shape factor and hydraulic conductance in noncircular capillaries I. One-phase creeping flow. *Journal of Colloid and Interface Science*, *304*(2), 295–304. https://doi.org/10.1006/jcis.2000.7413

Piri, M., & Karpyn, Z. T. (2007). Prediction of fluid occupancy in fractures using network modeling and X-ray microtomography. II: Results. *Physical Review E*, *76*(1), 016316. https://doi.org/10.1103/PhysRevE.76.016316

Prodanovic, M., Bryant, S. L., & Karpyn, Z. T. (2010). Investigating matrix/fracture transfer via a level set method for drainage and imbibition. *SPE Journal*, *125*(01), 125–136. https://doi.org/10.2118/116110-pa

Rabbani, A., Babaei, M., & Javadpour, F. (2020). A Triple Pore Network Model (T-PNM) for gas flow simulation in fractured, micro-porous and meso-porous media. *Transport in Porous Media*, *132*(3), 707–740. https://doi.org/10.1007/s11242-020-01409-w

Rabbani, A., Jamshidi, S., & Salehi, S. (2014). An automated simple algorithm for realistic pore network extraction from micro-tomography images. *Journal of Petroleum Science and Engineering*, *123*, 164–171. https://doi.org/10.1016/J.PETROL.2014.08.020

Rabot, E., Wiesmeier, M., Schlüter, S., & Vogel, H. J. (2018). Soil structure as an indicator of soil functions: A review. *Geoderma*, *314*, 122–137. https://doi.org/10.1016/j.geoderma.2017.11.009

Raeini, A. Q., Bijeljic, B., & Blunt, M. J. (2017). Generalized network modeling: Network extraction as a coarse-scale discretization of the void space of porous media. *Physical Review E*, *96*(1), 013312. https://doi.org/10.1103/PhysRevE.96.013312

Raeini, A. Q., Blunt, M. J., & Bijeljic, B. (2012). Modelling two-phase flow in porous media at the pore scale using the volume-of-fluid method. *Journal of Computational Physics*, *231*(17), 5653–5668. https://doi.org/10.1016/j.jcp.2012.04.011

Ramstad, T., Øren, P.-E., & Stig, B. (2010). Simulation of two-phase flow in reservoir rocks using a Lattice Boltzmann method. *SPE Journal*, *15*(04), 917–927. https://doi.org/10.2118/124617-pa

Rouchier, S., Janssen, H., Rode, C., Woloszyn, M., Foray, G., & Roux, J. J. (2012). Characterization of fracture patterns and hygric properties for moisture flow modelling in cracked concrete. *Construction and Building Materials*, *34*, 54–62. https://doi.org/10.1016/j.conbuildmat.2012.02.047

Sarkar, S., Toksöz, M. N., & Burns, D. R. (2004). *Fluid flow modeling in fractures*. Massachusetts Institute of Technology. Earth Resources Laboratory. Retrieved from http://hdl.handle.net/1721.1/68616

Schindelin, J., Arganda-Carreras, I., Frise, E., Kaynig, V., Longair, M., Pietzsch, T., et al. (2012). Fiji: An open-source platform for biological-image analysis. *Nature Methods*, *9*(7), 676–682. Retrieved from https://www.nature.com/articles/nmeth.2019

Scott, G. (2020). *Multiscale image based pore space characterisation and modelling of North Sea sandstone reservoirs (unpublished doctoral dissertation)*. University of Aberdeen.

Scott, G., Wu, K., & Zhou, Y. (2019). Multi-scale image-based pore space characterisation and pore network generation: Case study of a North Sea sandstone reservoir. *Transport in Porous Media*, *129*(3), 1–30. https://doi.org/10.1007/s11242-019-01309-8

Ushizima, D., Morozov, D., Weber, G. H., Bianchi, A. G., Sethian, J. A., & Bethel, E. W. (2012). Augmented topological descriptors of pore networks for material science. *IEEE Transactions on Visualization and Computer Graphics*, *18*(12), 2041–2050. https://doi.org/10.1109/TVCG.2012.200

Valvatne, P. H., & Blunt, M. J. (2004). Predictive pore-scale modeling of two-phase flow in mixed wet media. *Water Resources Research*, *40*(7), 1–21. https://doi.org/10.1029/2003WR002627

Wang, C. (2020). "Data for "Improvements to the fracture pipe network model for complex 3D discrete fracture networks"" (V2) [Dataset]. Mendeley Data. https://doi.org/10.17632/c8r645tj9v.2

Wang, C., Wu, K., & Scott, G. (2022). Improvements to the fracture pipe network model for complex 3D discrete fracture networks. *Water Resources Research*, *58*(3), e2020WR029450. https://doi.org/10.1029/2020WR029450

Wang, C., Wu, K., Scott, G. G., Akisanya, A. R., Gan, Q., & Zhou, Y. (2020). A new method for pore structure quantification and pore network extraction from SEM images. *Energy and Fuels*, *34*(1), 82–94. https://doi.org/10.1021/acs.energyfuels.9b02522

Weishaupt, K., Joekar-Niasar, V., & Helmig, R. (2019). An efficient coupling of free flow and porous media flow using the pore-network modeling approach. *Journal of Computational Physics X*, *1*, 100011. https://doi.org/10.1016/j.jcpx.2019.100011

Witherspoon, P. A., Wang, J. S., Iwai, K., & Gale, J. E. (1980). Validity of Cubic Law for fluid flow in a deformable rock fracture. *Water Resources Research*, *16*(6), 1016–1024. https://doi.org/10.1029/WR016i006p01016

Wu, K., Van Dijke, M. I. J., Couples, G. D., Jiang, Z., Ma, J., Sorbie, K. S., et al. (2006). 3D stochastic modelling of heterogeneous porous media – Applications to reservoir rocks. *Transport in Porous Media*, *65*(3), 443–467. https://doi.org/10.1007/s11242-006-0006-z

Wu, P., Li, Y., Sun, X., Liu, W., & Song, Y. (2020). Pore-scale 3D morphological modeling and physical characterization of hydrate-bearing sediment based on computed tomography. *Journal of Geophysical Research: Solid Earth*, *125*(12). https://doi.org/10.1029/2020JB020570